Impact of capillary flow hydrodynamics on carrier-mediated transport of opioid derivatives at the blood-brain barrier, based on pH-dependent Michaelis-Menten and Crone-Renkin analyses

Siti R. Yusof, N. Joan Abbott, Alex Avdeef

PII: S0928-0987(17)30350-0
DOI: doi: 10.1016/j.ejps.2017.06.016
Reference: PHASCI 4101

To appear in: *European Journal of Pharmaceutical Sciences*

Received date: 9 January 2017
Revised date: 10 April 2017
Accepted date: 9 June 2017

Please cite this article as: Siti R. Yusof, N. Joan Abbott, Alex Avdeef , Impact of capillary flow hydrodynamics on carrier-mediated transport of opioid derivatives at the blood-brain barrier, based on pH-dependent Michaelis-Menten and Crone-Renkin analyses, *European Journal of Pharmaceutical Sciences* (2017), doi: 10.1016/j.ejps.2017.06.016

Impact of capillary flow hydrodynamics on carrier-mediated transport of opioid derivatives at the blood-brain barrier, based on *pH*-dependent Michaelis-Menten and Crone-Renkin analyses

Siti R. Yusof [a], N. Joan Abbott [b], Alex Avdeef [c,*]

[a] HICoE Centre for Drug Research, Universiti Sains Malaysia, 11800 Minden, Penang, Malaysia

[b] King's College London, Institute of Pharmaceutical Science, Franklin Wilkins Building, 150 Stamford St., London SE1 9NH, UK

[c] *in-ADME* Research, 1732 First Avenue, #102, New York, NY 10128, USA

* Corresponding author at: *in-ADME* Research, 1732 First Avenue, #102, New York, NY 10128, USA.

Tel.: +1 646 678 5713. E-mail: alex@in-ADME.com (A. Avdeef)

ABSTRACT

Most studies of blood-brain barrier (BBB) permeability and transport are conducted at a single *pH*, but more detailed information can be revealed by using multiple *pH* values. A *pH*-dependent biophysical model was applied to the mechanistic analysis of published *pH*-dependent BBB luminal uptake data from three opioid derivatives in rat: pentazocine (Suzuki *et al*., 2002a, 2002b), naloxone (Suzuki *et al*., 2010a), and oxycodone (Okura *et al*., 2008). Two types of data were processed: *in situ* brain perfusion (ISBP) and brain uptake index (BUI). The published perfusion data were converted to apparent luminal permeability values, P_{app}, and analyzed by the *p*CEL-X program (Yusof *et al.* 2014), using the *pH*-dependent Crone-Renkin equation (*pH*-CRE) to determine the impact of cerebrovascular flow on the Michaelis-Menten transport parameters (Avdeef and Sun, 2011). For oxycodone, the ISBP data had been measured at *pH* 7.4 and 8.4. The present analysis indicates a 7-fold lower value of the cerebrovascular flow velocity, F_{pf}, than that expected in the original study. From the pyrilamine-inhibited data, the flow-corrected passive intrinsic permeability value was determined to be $P_0 = 398 \times 10^{-6}$ cm·s^{-1}. The uptake data indicate that the *neutral* form of oxycodone is affected by a transporter at *pH* 8.4. The extent of the cation uptake was less certain from the available data. For pentazocine, the brain uptake by the BUI method had been measured at *pH* 5.5, 6.5, and 7.4, in a concentration range 0.1 - 40 mM. Under similar conditions, ISBP data were also available. The *pH*-CRE determined values of F_{pf} from both methods were nearly the same, and were smaller than the expected value in the original publication. The transport of the cationic pentazocine was not fully saturated at *pH* 5.5 at 40 mM. The transport of the neutral species at pH 7.4 appeared to reach saturation at 40 mM pentazocine concentration, but not at 12 mM. In the case of naloxone, a *pH*-dependent Michaelis-Menten equation (*pH*-MME) analysis of the data indicated a smooth sigmoidal transition from a higher capacity uptake process affecting cationic naloxone (*pH* 5.0 - 7.0) to a lower capacity uptake process affecting the neutral drug (*pH* 8.0 - 8.5), with cross-over point near *pH* 7.4. Evidently, measurements at multiple *pH* values can reveal important information about both cerebrovascular flow and BBB transport kinetics.

KEY WORDS: blood-brain barrier; rodent *in situ* brain perfusion; brain permeability-surface area; *pH*-dependent Crone-Renkin equation; *pH*-dependent Michaelis-Menten analysis

Abbreviations

ABL	aqueous boundary layer adjacent to the cell surface (including glycocalyx)
CM/PD	carrier-mediated (saturable) / lipoidal passive diffusion (non-saturable)
D_{aq}	aqueous diffusivity ($cm^2.s^{-1}$)
F_{pf}	cerebrovascular flow velocity of perfusion/injection fluid ($mL{\cdot}s^{-1}{\cdot}g^{-1}$)
F(r/R)	Renkin molecular sieving function, dimensionless fraction in the range of 0 to 1
h_{ABL}	ABL thickness (cm)
ISBP/BUI	*in situ* brain perfusion/brain uptake index
J_{max}	maximum transport rate ($\mu mol{\cdot}min^{-1}{\cdot}g^{-1}$) of the saturable uptake process in the MM equation
k_d	the non-saturable uptake first-order rate constant ($mL{\cdot}min^{-1}{\cdot}g^{-1}$)
K_{in}	unidirectional transfer constant ($mL{\cdot}s^{-1}{\cdot}g^{-1}$); cf., Eq. (B.3)
K_m	half-saturation concentration (mM) Michaelis constant in the MM equation
MM	Michaelis-Menten; cf., Eq. (B.6)
pH-CRE	*pH*-dependent Crone-Renkin equation flow correction method
pH-MME	*pH*-dependent Michaelis-Menten equation analysis
P_{app}	*in vitro/in vivo* (planar/capillary) apparent permeability ($cm{\cdot}s^{-1}$); cf., Eq. (A.1) or (B.8)
P_C	corrected-for-flow (or -for-ABL) permeability coefficient ($cm{\cdot}s^{-1}$); depends on *pH* for ionizable permeants (hyperbolic function); basis of the *pH*-partition hypothesis; cf., Eq. (A.2)
P_i	flow-corrected luminal permeability coefficient ($cm{\cdot}s^{-1}$) of the *ionized* form of drug (carrier-mediated process); depends on *pH* for ionizable permeants (hyperbolic function); cf., Eq. (B.9)
P_+	maximum permeability in the P_i - *pH* curve ($cm.s^{-1}$)
P_0	maximum permeability in the P_C - *pH* curve: *in vitro/in vivo* intrinsic permeability of uncharged permeant ($cm.s^{-1}$)
P_{para}	paracellular permeability ($cm.s^{-1}$); cf., Eq. (A.3)
PS	permeability-surface area product ($mL{\cdot}s^{-1}{\cdot}g^{-1}$), traditionally determined from K_{in} using Crone-Renkin equation; cf., Eq. (B.5)
r	hydrodynamic molecular radius (Å)
R	effective cell layer junctional pore radius (Å)
S	endothelial surface area in a gram of brain tissue (100 $cm^2{\cdot}g^{-1}$ assumed in the calculations)
ε/δ	porosity of paracellular junction pores divided by the rate-limiting paracellular pathlength (size-restricted, cation-selective)
$(\varepsilon/\delta)_2$	secondary porosity-pathlength ratio (charge/size nonspecific “free diffusion” term)
$\Delta\varphi$	electrical potential drop (mV) across the electric field created by negatively-charged residues lining the junctional pores

1. Introduction

The relationship between membrane permeability and *pH* can reveal the extent of the contribution from several effects relevant to drug absorption/distribution, such as aqueous boundary layer (ABL) resistance, paracellular leakage, and drug ionization (Ho *et al*., 2000), including those related to carrier-mediated/facilitated transport (Thomson and Dietschy, 1977; Tsuji *et al*., 1994; Takanaga *et al*., 1994).

The mammalian intestinal barrier (Wilson, 1967; Högerle and Winne, 1983; Kararli, 1995; Collett *et al.,* 1997; Desesso and Williams, 2008) possesses variable *pH* gradients (acidic on the luminal side, neutral on the blood side). So, it is not so uncommon to find studies of drug transport as a function of *pH* – most obviously, to mimic the physiological *pH* conditions, but more subtly, to tease out contributions to transport from several biophysical factors (Ho *et al*., 2000). For example, there have been many published *in vitro* studies using cell lines (*e.g.*, Caco-2, MDCK), or primary cell cultures (*e.g.*, porcine brain capillary endothelium), where permeability was measured at two different *pH* values in the interval 5.4-7.4, under gradient-*pH* and/or iso-*pH* conditions (Adson *et al.,* 1995; Pade and Stavchansky, 1997; Raeissi *et al.,* 1999; Yamashita *et al*., 2000; Laitinen *et al.,* 2003; Alsenz and Haenel, 2003; Lee *et al.,* 2005; Bhardwaj *et al.,* 2005; Berginc *et al.,* 2007; Kanaan *et al.,* 2008). A few studies have been published where 3-4 different *pH* values were considered (Takanaga *et al*., 1994; Yu and Zeng, 2007; Agarwal *et al.,* 2007; Korjamo *et al.,* 2008; Yusof *et al.,* 2014). The most comprehensive *in vitro* investigations, with up to nine different *pH* values per molecule considered, were reported by Artursson and coworkers (Palm *et al.,* 1999; Neuhoff *et al.,* 2003, 2005; Avdeef *et al.,* 2005). Principally, these *pH*-dependent studies focused on modeling the intestinal barrier, with one exception (Yusof *et al.,* 2014). Controls were included in the assays to confirm that the biological barrier stayed intact as a result of *pH* changes.

In contrast to the intestinal environment, the *in vivo* blood-brain barrier (BBB) has no appreciable *pH* gradient between the luminal and the abluminal sides. It may not appear obvious that *in vivo* studies of BBB permeability as a function of *pH* have any practical relevance. Indeed, there could be concern that non-physiological *pH* might disrupt the tightly-regulated BBB. As it turns out, the BBB can withstand a range of *pH* values, *provided the exposure time is short*. For example, Greenwood *et al.* (1989) saw no significant mannitol permeability increase when a *pH* 5.5 lactic acid solution was perfused through rat brain for 450 s. In the 30-s *in situ* rat brain perfusion study of several highly lipophilic drugs (amitriptyline, atomoxetine, imipramine, maprotiline, sertraline, indomethacin) in *pH* 5.5-8.5 buffers, physical integrity of the BBB was confirmed using markers (moderately permeable antipyrine and low-permeable atenolol) co-perfused in the sample-containing buffers (Avdeef and Sun, 2011).

With the possible opportunities to deconvolve/quantify several factors affecting BBB transport (*e.g.*, impact of cerebral perfusion fluid flow on assessment of lipophilic drug uptake, native/disease-state paracellular leakage, carrier-mediated/facilitated effects), surprisingly only a hand-full of *pH*-dependent *in vivo* studies of transport at the BBB have been reported (Suzuki *et al.,* 2002a, 2002b, 2010a; Okura *et al.,* 2008; Avdeef and Sun, 2011; Suzuki *et al.,* 2016). Efficient computational tools to comprehensively evaluate such *pH*-dependent data have not been widely applied (Yusof *et al*., 2014).

In this study, we exploit what has been learned from the *pH*-dependent *in vitro* cell-based biophysical models (sharpened by intestinal applications), and apply such models to the novel mechanistic analysis of the published *pH*-dependent *in vivo* data for pentazocine (Suzuki *et al*., 2002a, 2002b), naloxone (Suzuki

et al., 2010a), and oxycodone (Okura *et al*., 2008), to illustrate the potential value of *pH* modulation for *in vivo* BBB assays. Preliminary treatment of oxycodone data has been described (Avdeef and Sun, 2010). In the case of naloxone, a *pH*-dependent Michaelis-Menten equation (*pH*-MME) analysis indicated a smooth sigmoidal transition from a cation CM uptake process (*pH* 5.5-7.0) to a neutral-species CM uptake process (*pH* 8.0-8.5), with near equal contribution from both types at *pH* 7.4. The *p*CEL-X program (Yusof *et al.,* 2014) used in the study was further expanded to accommodate new computational features related to carrier-mediated (CM) transport.

2. Materials and methods

2.1. Data sources

The data used here to illustrate the impact of capillary flow hydrodynamics on carrier-mediated transport of the opioid derivatives were from Suzuki *et al.* (2002a, 2002b, 2010a) and Okura *et al.* (2008). Table 1 lists the physicochemical properties of the three drugs studied. Table 2 lists the data taken from the original sources, but converted to capillary-based apparent permeability values as a function of *pH*.

2.2. Biophysical model

In vitro cell monolayers grown to confluence on porous filters have been used to model drug absorption properties of the *in vivo* cell membrane barriers. Such models factor in a number of effects, including (i) the resistance of the aqueous boundary layer (ABL) at the interface between the aqueous solution and the cell surface, (ii) the paracellular leakiness of the cell junctions, and (iii) the pH of the solution. Appendix A describes the equations applied to *in vitro* cell monolayer data analyses. Appendix B extends the construct to *in vivo* models of uptake at the BBB from perfusate/injectate flow in brain capillaries.

By way of introduction to the computational approach, a simple electrical circuit may be considered. In the circuit analogy, resistance and permeability are related inversely. In a *series circuit*, the total resistance is the sum of the individual resistances. In a *parallel circuit*, the total permeability is the sum of the permeabilities of each parallel path. For example, consider that a molecular transport barrier consists of three lamellae: (a) luminal aqueous boundary layer (ABL1), (b) layer of cells bound together *very tightly* (CELL), and (c) abluminal aqueous boundary (ABL2). The total resistance to transport would be: $R_{TOT} = R_{ABL1} + R_{CELL} + R_{ABL2}$. In permeability terms, $1/P_{TOT} = 1/P_{ABL1} + 1/P_{CELL} + 1/P_{ABL2}$. Usually, the measured ABL permeability implicitly includes both ABL layers (since it is difficult to measure individual contributions), as $1/P_{ABL} = 1/P_{ABL1} + 1/P_{ABL2}$. Next, consider a cell barrier with *leaky* junctions, so that there are two parallel paths a molecule may take: paracellular (para) and transcellular (C). In permeability terms, $1/P_{TOT} = 1/P_{ABL} + 1/(P_C + P_{para})$. This simple analogy is the basis for the biophysical model described here, as elaborated in the appendices.

So, when a diffusion path is in *series* through several sequential diffusion barriers (*e.g.*, aqueous

boundary layer plus a cell monolayer), the total *inverse* permeability is the sum of the individual inverse permeabilities. This is denoted by Eq. (A.1) in Appendix A. The last term in Eq. (A.1) exemplifies *parallel* resistances, where permeability is additive. This is where the same diffusion layer has contiguous patches of different permeability (*e.g.*, transcellular plus paracellular paths). Figure 1 illustrates a typical plot of logarithmic permeability as a function of *pH*. The *in vitro* and *in vivo* curves are very similar. The caption in Figure 1 describes the different components. The filter contribution, which would be relevant only to the *in vitro* case, is not shown. The filter permeability curve would be a line parallel to the ABL permeability line, but above it as in the case of translucent polycarbonate filters, but not necessarily of clear plastic polyethylene filters (Yusof *et al.,* 2014).

As can be seen in Figure 1, the apparent permeability of ionizable molecules depends on *pH*, and the shapes of the permeability-*pH* profiles can be theoretically predicted when the pK_a of the molecule is known, the *pH*-partition hypothesis is valid, and the resistance of the ABL is not neglected. There are opportunities to apply some elements of these planar biophysical models to study the drug penetration properties in the capillary environment of the blood-brain barrier (BBB). The appendices summarize the computational details underpinning the case studies described in the *Results and discussion* section.

In the rodent *in situ* brain perfusion (ISBP) technique, the traditional method used to determine cerebral blood flow rate, F_{pf} (cf., Eq. (B.3)), of highly permeable compounds is based on the flow marker diazepam (Takasato *et al.,* 1984; Smith, 2003). Sometimes uptake studies are reported with cerebral blood flow F_{pf} values taken from earlier published studies, with the assumption that once determined, the values are re-usable in subsequent studies in the same animal model.

An alternative method for correcting for cerebral flow was developed by Avdeef and Sun (2011). Provided that K_{in} (cf., Eq. (B.3)) values are determined at several values of perfusate *pH*, the highly-permeable drug *itself* can serve as a flow marker, in a procedure described as the *pH*-dependent Crone-Renkin (*pH*-CRE) method in Appendix B.

2.3. Computational tool for in vitro/in vivo permeability analysis

A weighted nonlinear regression method (Avdeef, 2012; Yusof *et al.,* 2014) was used to analyze the terms in the planar monolayer Eq. (A.1) and the capillary flow Eq. (B.10). The *p*CEL-X v4.0 program (*in-ADME* Research) was used to determine the Michaelis-Menten parameters J_{max}, K_m, and k_d (using experimentally weighted data – see *Abbreviations* for definitions of terms), and the paracellular parameters ε/δ, $(\varepsilon/\delta)_2$, R, $\Delta\varphi$ and h_{ABL} (which apply to both planar and capillary cases), based on the logarithmic form of Eq. (A.1). The program was also used to determine the F_{pf}, P_0 and, where possible, P_+ *or* P_{para} (but not both) by the capillary flow *pH*-CRE method (Eq. (B.10)). The analytical partial derivatives of the log K_{in} unidirectional transfer function with respect to the refinable parameters F_{pf}, P_0, P_i, and P_{para} are calculated explicitly, based on standard mathematical techniques. The function minimized during refinement is the sum of weighted residuals, as previously described (Avdeef, 2012). The goodness-of-fit (GOF), the root-mean-square of the minimized function, is used as a quality of fit index. Ideally, GOF has the expectation value of 1.0 if the experimental errors in the dependent variables used in the regression are reliable (and scaled accordingly) and the model is appropriate.

2.4. Assumptions made

The opioids considered here show complicated uptake mechanisms at the BBB, involving carrier-mediation (CM) as well as lipoidal passive diffusion (PD). The analyses presented here draw on the assumptions: (i) uptake into the brain (across the BBB) can involve both CM and PD processes; (ii) in the PD process, the *pH* partition hypothesis is valid, namely, that only the neutral species can cross the BBB (*i.e*., cationic opioids assumed not to cross the BBB by PD); (iii) for the lipophilic opioids, paracellular transport is inconsequential at the BBB (due to the tight junctions); (iv) the ABL resistance is negligible under brain capillary fluid flow conditions; (v) the lipophilic opioids cannot permeate the BBB, either by PD or CM, at a velocity greater than that of the cerebral capillary fluid flow (*i.e.*, $K_{in} \leq F_{pf}$); (vi) the effect of efflux is not explicitly considered (*i.e.,* where possible, data with very low injectate/perfusate concentrations were excluded in the MM analyses).

3. Results and discussion

3.1. Oxycodone cerebral blood flow rate from pH-dependent Crone-Renkin equation (pH-CRE)

A case study in *pH* dependence at the BBB is illustrated by the opioid agonist, oxycodone (Okura *et al.* 2008). There is evidence that the drug is subject to carrier-mediated uptake by the pyrilamine transporter, a putative organic cation energy-dependent H^+-coupled antiporter. The rat ISBP data were measured at a flow rate of 4.9 mL·min^{-1}, at both *pH* 7.4 and 8.4, with uptake determined at several time points over a 30-s interval. Since the cerebral flow rate was not available in the study, the authors used an earlier-published value, F_{pf} = 0.1256 mL·s^{-1}·g^{-1} (Takasato *et al*., 1984). This cerebral flow rate suggests that oxycodone uptake would not be flow-limited in the perfusion experiment (*i.e*., based on the above F_{pf}, log (F_{pf}/S) = -2.90 is well above the highest point in Fig. 2). However, since K_{in} values were measured at two different *pH* values in the Okura *et al.* study, the data could be re-analyzed by the new *pH*-CRE method.

Figure 2 shows the results of such an analysis. An accurately measured pK_a 8.73 of oxycodone at 37 ^{o}C was used (Table 1). Oxycodone is 96% and 68% positively charged at *pH* 7.4 and 8.4, respectively. For the inhibited and uninhibited cases in the figure, the *pH*-CRE F_{pf} values (represented by the dotted lines) are nearly identical, and are 7-fold lower than the assumed value.

In Figure 2, the upper curve with the circle symbols represents the perfusion-derived log P_{app} as a function of *pH* in the absence of inhibitors. The *apparent* intrinsic permeability is 908 x 10^{-6} cm·s^{-1}. This is the value determined using Eq. (B.10) applied to the two measurements done in the *absence* of inhibitor, and includes contributions from both CM and PD processes. If F_{pf} = 0.1256 mL·s^{-1}·g^{-1} is used in place of the determined value (0.020 mL·s^{-1}·g^{-1}), then the apparent intrinsic value decreases to 574 x 10^{-6} cm·s^{-1}.

In the presence of 1 mM pyrilamine (as inhibitor), the permeability decreases at both *pH*, as indicated by the curve with the square symbols, confirming that oxycodone is a substrate of a pyrilamine transporter. The purely passive intrinsic permeability value was determined to be 398 x 10^{-6} cm·s^{-1}

(= log P_0 -3.40 from Eq. (B.10) applied to the two points measured in the presence of inhibitor). If F_{pf} = 0.1256 mL·s^{-1}·g^{-1} is used in place of the determined value (0.016 mL·s^{-1}·g^{-1}), then the intrinsic value decreases to 354 x 10^{-6} cm·s^{-1}. The difference between the two P_0 values is not big because the apparent permeability values are well below the flow limit in the inhibited case.

If one assumes that CM transport contribution is entirely eliminated by 1 mM pyrilamine, the analysis by the *pH*-CRE method suggests that in the absence of inhibitor, a CM process increases the permeability of the *uncharged* species by a factor of 2.3 (=908/398), implying that the transporter appears to facilitate the uptake of the *neutral* form of the drug. This is suggested by the *parallel* displacement of the two curves in the pH 7.4-8.4 interval as the result of added inhibitor. Given that the pK_a of oxycodone is 8.73, it was not possible to fit the *pH* 7.4 and 8.4 data with permeability coefficient of the cationic species (P_+). Consequently, the action of the transporter on the *cationic* form of oxycodone is not definitive, even though in the *pH* range examined, 68 - 96% of the drug is in the charged form. An expanded range of *pH* data, particularly down to *pH* 5.5 (*e.g.*, as with naloxone example below) would be needed to directly address the uptake of the *charged* form of oxycodone.

3.2. Pentazocine cerebral blood flow rate from pH-dependent Crone-Renkin equation (pH-CRE) applied to Michaelis-Menten analysis

Pentazocine is a lipophilic (log *P* 3.31, Yokogawa *et al.,* 1990) narcotic-antagonist (potent non-addictive analgesic). Two types of rat data are available: (a) carotid injection brain uptake index, BUI (Suzuki *et al.,* 2002a), and (b) ISBP (Suzuki *et al.,* 2002b). The opioid is taken up into the brain by an influx transporter mechanism, which can be inhibited by pyrilamine and naloxone (Suzuki *et al.,* 2002a, 2002b). Rodent brain uptake data from the two different methods vs. *pH* afforded a way to determine the cerebral capillary flow velocity *in situ* (*i.e.,* pentazocine served as its own flow marker). This newly-determined flow velocity was then applied to the Michaelis-Menten re-analysis of uptake fluxes vs. concentration in the pH 5.5-7.4 interval. Critical to the analysis was the availability of reliably measured pK_a values at 37 ^{o}C. The two values used here (Table 1) were determined by analysis of the 23 ^{o}C solubility data (Wilson, 1984), followed by conversion to the physiological temperature (Sun and Avdeef, 2011). Pentazocine is 100% and 98% positively charged at *pH* 5.5 and 7.4, respectively. Since the P_{para} predicted by *p*CEL-X for pentazocine is 0.08 x 10^{-6} cm·s^{-1} at the rodent blood-brain barrier (Avdeef, 2012), paracellular drug diffusion was not considered here.

3.2.1 BUI pentazocine data

Figure 3a shows the BUI uptake from a 0.1 mM injectate solution at *pH* 5.5, 6.5, and 7.4 (circles). Also, BUI uptake was measured from 40 mM solutions at pH 5.5 and 7.4 (squares). Brain concentrations were determined at the end of 15-s injection time (Suzuki *et al.,* 2002a).

To test the impact of a re-determined F_{pf} on the uptake kinetics in the BUI method, it was necessary to re-calculate the mean capillary concentrations and the flux values in the Suzuki *et al.* (2002a) study (*J* vs. C_{cap} in their published Fig. 3 at *pH* 5.5 and Fig. 1b at *pH* 7.4), as described in Sec. 3.3.

The BUI% values for 0.1 mM injection solutions (C_{inj}) at *pH* 5.5, 6.5, and 7.4 (Fig. 2 in Suzuki *et al.,* 2002a) were converted to K_{in} (mL·s^{-1}·g^{-1}) values (cf., Appendix B). The K_{in} vs. pH values were subjected to *p*CEL-X analysis, to obtain three *pH*-CRE parameters: F_{pf}, P_0, and P_+ (cf., *Abbreviations*). The cerebral capillary flow rate was calculated to be F_{pf} = 0.0082 mL·s^{-1}·g^{-1}. This value is smaller than the legacy value applied by Suzuki *et al*. (0.0155 mL·s^{-1}·g^{-1} from Pardridge and Fierer, 1985). The *apparent* intrinsic permeability (at 0.1 mM) was determined to be 13 x 10^{-3} cm·s^{-1}(log S_0 -1.90), which is a higher value than that expected of a passive diffusion process (~3.3 x 10^{-3} cm·s^{-1} by *p*CEL-X *in situ* brain intrinsic permeability prediction), suggesting that a CM process contribution might be substantial at 0.1 mM. The apparent cationic species permeability, P_+, was determined to be 18 x 10^{-6} cm·s^{-1} (cf., Eq. (B.10)).

At 0.1 mM C_{inj}, the uptake appears to be flow limited (K_{in} nearly equals the determined F_{pf} in the upper solid curve at *pH* 7.4, Fig. 3a). At 0.1 mM injectate, it was assumed that efflux did not affect the calculation of F_{pf} at pH 7.4. At an even lower 0.02 µM perfusate concentration in the ISBP data (below), nearly the same value of F_{pf} was calculated, which suggests that the efflux contribution was relatively small and did not reduce the K_{in} below the estimated flow limit. (A measurement *at* pH 8.0 would have made the above interpretation more certain.) To examine the *pH*-dependent uptake under presumably saturating conditions, the BUI% values at the maximum concentration (C_{inj} 40 mM) at *pH* 5.5 and 7.4 (Suzuki *et al*. 2002a Figs. 1a and 3, resp.) were also subjected to the *pH*-CRE analysis. Since only two-*pH* data were reported, only two parameters could be determined. At 40 mM, the reported permeability values at *pH* 5.5 and 7.4 were not flow-limited (the limit is reached only for pH > 8.7, lower solid curve in Fig. 3a). Consequently, the F_{pf} value from the three-point (0.1 mM) calculation was included as a fixed contribution in the 40 mM injectate case, so that P_0 and P_+ could be determined. The intrinsic and the cationic permeability values under the potentially saturating conditions (lower solid curve in Fig. 3a) were determined as P_0 = 838 x 10^{-6} (log P_0 -3.08) and P_+ =10 x 10^{-6} cm·s^{-1}, respectively.

Figure 3a depicts the results of the *pH*-CRE analysis. At the 40 mM concentration, the neutral-species CM transport is apparently saturated. This can be surmised from the Michaelis-Menten (MM) analysis of the flow-corrected flux (*J*) vs. mean capillary concentration (C_{cap}) data (cf., Sec. 3.3), where the non-saturable permeability was determined to be k_d = 0.030 mL·min^{-1}·g^{-1} at *pH* 7.4 (Fig. 4b and Table 3), which converts to P_C = 5 x 10^{-6} cm·s^{-1}. The uncertainty in this value is relatively high, due to the scatter of points in Figure 4b. For example, if the two highest concentration points in Figure 4b were not used in the MM regression analysis, then the resultant k_d = 0.155 mL·min^{-1}·g^{-1}, which converts to P_C = 26 x 10^{-6} cm·s^{-1}. In Figure 3a, the lower dashed curve evaluated at pH 7.4 indicates P_C = 16 x 10^{-6} cm·s^{-1}. Since the latter value is between the above bounding k_d values (5 and 26 x 10^{-6} cm·s^{-1}), it may be concluded that at 40 mM injectate concentration level, the uptake process predominantly reflects the *passive* permeability of the uncharged pentazocine, associated with the intrinsic permeability value of log P_0 = -3.08.

Given that the CM process is saturated for the neutral species at 40 mM injectate concentration, the above passive diffusion intrinsic permeability, P_0, can be transformed to non-saturable permeability coefficients, k_d, at *pH* 7.4 (0.098 mL·min^{-1}·g^{-1}) and *pH* 5.5 (0.0013 mL·min^{-1}·g^{-1}). These *passive* lipoidal values are not expected to be affected by the transporter process. However, the MM analyses of the *pH* 7.4 and 5.5 flux-concentration data indicate different values (0.03 and 0.05 mL·min^{-1}·g^{-1}, resp.; cf., Table 3). Such differences appear to be at odds with the assumptions made in Sec. 2.4, as discussed

below.

It is interesting to note that the weighted MM nonlinear regression analysis to determine the J_{max}, K_m, and k_d constants indicates very high correlations between these parameters. For example, at *pH* 7.4: J_{max} and K_m, are 95% positively correlated; J_{max} and k_d are 96% negatively correlated; K_m and k_d are 88% negatively correlated. This suggests that the constants are not so uniquely determined and that a range of possible solutions can nearly equally fit the same data. A possible remedy is to refine fewer than three parameters, even though the GOF may increase slightly. We tested this by setting the k_d parameter calculated from the P_0 determined by the *pH*-CRE analysis of the 40 mM data, taking into account the *pH* dependence (cf., Eq. (A.2)). The k_d was not refined, however. So, only the J_{max} and K_m parameters were determined by regression. At *pH* 7.4, the J_{max} and K_m decreased from 4.6 to 2.7 µmol·min^{-1}·g^{-1} and 3.3 to 1.4 mM, respectively, as a result of fixing the k_d to 0.098 mL·min^{-1}·g^{-1} (BUI method, Table 3). The ISBP data showed slight increases in the two refined parameters (Table 3). Notably, the goodness-of-fit increased from 0.9 to 1.8 (BUI) and from 2.9 to 3.9 (ISBP), as a consequence of entering the fixed value of k_d calculated from the *pH*-CRE P_0.

The MM-calculated k_d value at pH 7.4 would be expected to decrease at pH 5.5, if the non-saturable process involved solely the passive diffusion of the neutral species (cf., assumptions in Sec. 2.4). But in fact, it *increased* from 0.03 to 0.05 mL·min^{-1}·g^{-1} (BUI, Table 3). When the k_d (= 0.0013 mL·min^{-1}·g^{-1}) based on the *pH*-CRE P_0 was included as a *fixed* contribution in the *pH* 5.5 MM analysis, the K_m increased 17-fold from 2.4 mM to 40 mM, as J_{max} increased nine-fold from 0.5 to 4.7 µmol·min^{-1}·g^{-1}, compared to the values at pH 7.4. In effect, the dotted line (PD) in Figure 4a nearly merged with the horizontal axis, while the dashed (CM) curve nearly merged with the total flux solid curve. The GOF increased only by a small amount (0.8 to 1.1), suggesting that the fit was nearly as good with the fixed k_d (determined by the *pH*-CRE method) compared to when all three MM parameters are simultaneously determined. Section 3.4 further addresses the apparent limitations in the MM analysis applied to the pentazocine data.

3.2.2 ISBP pentazocine data

The ISBP data (Suzuki *et al.,* 2002b) were measured at a flow rate of 3.6 mL·min^{-1}, at *pH* 5.5, 6.5, and 7.4, with uptake determined at several time points over a 30-s interval. Figure 3b shows the data at 0.02 µM (three filled circles) and 12 mM (two filled squares). Using the *pH*-CRE method, the cerebral capillary flow rate was calculated as F_{pf} = 0.0091 mL·s^{-1}·g^{-1}, nearly the same value as determined from BUI data (Sec. 3.2.1), but still differing from the reported value of 0.0392 mL·s^{-1}·g^{-1}. The apparent intrinsic and cationic permeability values were calculated as 31 x 10^{-3} (log P_0 -1.51) and 40 x 10^{-6} cm·s^{-1}, respectively, at 0.02 µM concentration. At 12 mM concentration, the corresponding values were calculated as 1.6 x 10^{-3} (log P_0 -2.80) and 12 x 10^{-6} cm·s^{-1}, respectively. These values are consistent with those derived from the BUI data (cf., Figs. 3a and 3b). Figures 4c and 4d are based on the analysis of the ISBP data. The refined J_{max}, K_m, and k_d parameters are comparable to those obtained from the BUI data (Figs. 4a, 4b; Table 3).

3.2.3 Contribution of carrier-mediated process to overall uptake in the Michaelis-Menten relationship

In the limit of zero perfusate/injectate concentration, the MM equation, Eq. (B.6), may be restated in terms of limiting permeability values, as $J/C = J_{max}/K_m + k_d$. The J_{max}/K_m term refers to the limiting permeability due to the CM process. In Table 3, CM% is to the percentage of the CM contribution to the total permeability. In the BUI MM calculation with two refined parameters (k_d provided as a fixed contribution) at pH 5.5, 99% of the transport is attributable to the CM process. The value drops to 95% at *pH* 7.4. This is consistent with increased neutral-species permeation by PD as pH is raised. Pentazocine is 100% charged at pH 5.5 and 98% charged at pH 7.4, which suggests that the pentazocine cation is the predominant substrate for the transporter across the entire *pH* range studied. Even at the 40 mM injectate level, the CM uptake of the pentazocine cation in not fully saturated. Under these conditions, the neutral species only permeates by lipoidal passive diffusion.

3.3. Re-calculation of the pentazocine uptake curves (J vs. C_{cap}) as a result of the newly-determined F_{pf}

The procedure for extracting from the reported uptake data the legacy value of F_{pf} and replacing it with the value determined by the Crone-Renkin-*pH* analysis is described here for the *pH* 7.4 flux (J) vs. C_{cap} profile (Fig. 1b in Suzuki *et al.,* 2002a). The theoretical relationships used are described in Appendix B. First, the original C_{inj} values were digitized from the published Fig. 1a (BUI% vs. C_{inj}). Also, values of C_{cap}, J, and standard deviations (SD) were digitized from the published Fig. 1b (J vs. C_{cap}). The original flow-corrected *PS* values were calculated as J/C_{cap}. From these, the flow-uncorrected K_{in} values were determined using Eq. (B.3), where the assumed legacy value of F_{pf} = 0.0155 mL·s^{-1}·g^{-1} had been applied in the case of the BUI data. This, in effect, "de-corrected" the original uptake data for flow. The process was then reversed, with the calculation of the new *PS* values based on the new F_{pf} = 0.0082 mL·s^{-1}·g^{-1} determined by the *pH*-CRE analysis (BUI data). The new C_{cap}/C_{inj} ratio was calculated using Eq. (B.4). The product of this ratio and the C_{inj} values produced the new C_{cap} concentrations. The main effect of the flow parameter re-adjustment is to make the new C_{cap} values smaller than the original values; flux values were only barely altered, as indicated in Figures 4a and 4b. A similar flow de-correction/correction procedure was applied to the ISBP data, substituting the reported F_{pf} of 0.0392 mL·s^{-1}·g^{-1} with the *pH*-CRE value of 0.0091 mL·s^{-1}·g^{-1}.

3.4. Limitations in the Michaelis-Menten analysis

The inconsistencies between the k_d values calculated by the MM and the *pH*-CRE analyses may be due to the high correlations between the three refined MM parameters, and also of the way the MM equation is defined when ionizable molecules are considered. The concentration term in the MM equation, Eq. (B.6), does not explicitly specify the charge state of the ionizable drug evaluated. It is evident at *pH* 5.5 in Figure 3 that the cation is taken up by a saturable process (*i.e.,* K_{in} increases as concentration decreases). The points at *pH* 5.5 lie along the hyperbolic dash-dot cation species curves (CM only), and are well above the parabolic neutral species dashed curves at *pH* 5.5 (neutral species: CM and PD at 0.1 mM, but only PD at 40 mM). It is also evident from the *pH*-CRE analysis that the predicted dashed curves at pH 9.5 indicate a saturable process that affects the neutral species (apparent P_0

increases with decreasing drug concentration). Appendix B considers possible further expansions of the MM equation to take into account the ionization constants of the drug. The naloxone data below tested the idea of pH-dependent MM analysis.

3.5. Naloxone cerebral blood flow rate from pH-dependent Crone-Renkin equation (pH-CRE)

Naloxone is a potent opioid antagonist, which can permeate the BBB at nearly ten times the rate of morphine (Suzuki *et al.,* 2010a). A mechanism consisting of both passive diffusion and a CM uptake was proposed by the investigators. The saturable process is strongly inhibited by cationic H_1-antagonists, *e.g.,* pyrilamine. Unlike pentazocine considered above, naloxone is apparently not a substrate for P-gp (Suzuki *et al.,* 2010b). The moderately lipophilic ampholytic drug naloxone (log *P* 1.81, Kansy *et al.,* 2001), with pK_a 9.25 and 7.82 at 37 ^{o}C (Kaufman *et al.,* 1975), was critically examined by Suzuki *et al.* (2010a), using the BUI method. At *pH* 7.4, the flux at *ten* different concentrations (0.5 µM - 15 mM) was reported. In addition, 0.1 µM carotid artery injection (BUI) measurements were performed at *pH* 5.5, 6.0, 6.5, 7.0, 7.4, 8.0, and 8.5. Furthermore, 10 mM injection measurements were performed at *pH* 5.5, 6.0, 6.5, 7.0, and 7.4. As far as we are aware, this unique study represents the largest range of *pH* used for BBB permeability measurement in the literature. The data appear to be of high quality. Thus, there was an opportunity to extract additional insights into the nature of the rate of naloxone BBB penetration and how it depends on *pH*, by applying the *pH*-CRE and *pH*-MME analyses (cf., Appendix B).

The re-analysis started with the conversion of the BUI-*pH* data (Fig. 2 in Suzuki *et al*., 2010a) into log (K_{in}/S)-*pH* data format accepted by the *p*CEL-X program. It was possible to obtain three constants by the weighted regression procedure. For the 0.1 µM set: F_{pf} = 0.0055 ± 0.0001 mL·s^{-1}·g^{-1}, log P_0 = -3.69 ± 0.04 (cm·s^{-1}), and log P_+ = -4.41 ± 0.02 (cm·s^{-1}), GOF = 0.31, n = 7. For the 10 mM set: F_{pf} = 0.0055 ± 0.0001 mL·s^{-1}·g^{-1}, log P_0 = -3.98 ± 0.02 (cm·s^{-1}), and log P_+ = -4.59 ± 0.01 (cm·s^{-1}), GOF = 0.29, n = 5.

Figure 5 shows the best-fit (solid) curves for the two sets of data, with the filled circles and squares representing the 0.1 µM and 10 mM sets, respectively. The (flow-corrected) neutral-species (*pH*-partition hypothesis) log P_C parabolic curves are represented by short and long dashes for the 0.1 µM and 10 mM sets, respectively. The flow-corrected ionic-species log P_i hyperbolic curves are represented by the two dash-dot curves. The flow velocities refined to identical F_{pf} values for the two sets. These are indicated by the dotted horizontal line.

Next, the flux-concentration data (Fig. 1 in Suzuki *et al*., 2010a) were evaluated using the MM equation. The flux and mean capillary values were re-calculated according to the newly determined *pH*-CRE F_{pf} value, following a procedure similar to that described for pentazocine above (Sec. 3.3). Figure 6 shows the resultant Michaelis-Menten (MM) analysis at *pH* 7.4. The three parameters obtained by the weighted nonlinear MM analysis are J_{max} = 2.0 ± 0.9 µmol·min^{-1}·g^{-1}, K_m = 6.1 ± 2.0 mM, and k_d = 0.12 ± 0.05 mL·min^{-1}·g^{-1}; GOF = 2.5, n = 10.

The non-saturable k_d parameter obtained, 0.12 mL·min^{-1}·g^{-1}, was converted to the equivalent P_C value at *pH* 7.4, from which the whole log P_C curve was calculated, with knowledge of the pK_a values, and is shown in Figure 5 as the dash-dot-dot parabolic curve. Some interesting conclusions can be derived from

the inspection of Figure 5. The three parabolic curves have a systematic dependence on concentration, suggesting that the neutral ampholyte is a substrate for an influx transporter. At 10 mM concentration, the process is not entirely saturated, since the k_d-derived curve is lower than that indicated by the 10 mM data (middle parabolic curve). It is reasonable to assume that the intrinsic permeability derived from the MM analysis k_d, $P_0 = 74 \times 10^{-6}$ cm·s^{-1}, describes the passive transport process. This is not far from the *p*CEL-X prediction of the naloxone passive *in situ* brain perfusion, $P_0 \sim 256 \times 10^{-6}$ cm·s^{-1} (cf., Tsinman *et al.,* 2011).

3.6. Naloxone: pH-dependent Michaelis-Menten equation (pH-MME) analysis

Assuming that the passive intrinsic permeability, P_0, determined from the MM analysis k_d value from *pH* 7.4 data can be used to predict the k_d values at other *pH* values (cf., Eq. (A.2) and Sec. 2.4), it seemed possible that two-point Michaelis-Menten analysis could be used to determine J_{max} and K_m at each of the *pH* values from 5.5 to 8.5, provided a value of k_d (*pH*-dependent) is included as a fixed contribution at each *pH* in the MM analysis. The missing 10 mM data at *pH* 8.0, 8.5 were approximated according to the lower solid curve in Figure 5. The pH-MME procedure is further discussed in Sec. B.4.

Figure 7 summarizes such a *pH*-MME analysis. It appears that two uptake mechanisms may be operating across the *pH* range (Fig. 7a): a higher capacity uptake process affecting the naloxone cation in the range *pH* 5.0 -7.0 ($J_{max} \sim 3.2$ µmol·min^{-1}·g^{-1}, $K_m \sim 14$ mM) and a lower capacity uptake process affecting the neutral drug in the *pH* 8.0 - 8.5 range ($J_{max} \sim 0.5$ µmol·min^{-1}·g^{-1}, $K_m \sim 3$ mM). Consistent with this, the percentage of CM contribution (Fig. 7b) to the overall transport is greater in the region of the cationic transporter (*pH* 5.5) than that of the neutral transporter (*pH* 8.5). This can be interpreted as the action of a single transporter which has different specificities for the two charge forms of naloxone.

4. Conclusions

This study has shown that careful analysis of BBB permeability data, obtained from both *in situ* brain perfusion (ISBP) and carotid injection (BUI) techniques and using a range of experimental *pH*, can reveal important additional information not obvious from the original published reports. The computation tool *p*CEL-X was instrumental in the calculations involved, and the internal consistency of the analysis adds to evidence for the reliability and accuracy of the methods. Notable findings were improved estimates of F_{pf} for both ISBP and BUI, and resolution of CM components of permeability for all three compounds examined: oxycodone, pentazocine and naloxone.

It is clear from this *post hoc* analysis that even better understanding of underlying mechanisms would have been possible had the proposed experimental conditions been tested in advance (or at an early stage), using *p*CEL-X to establish the optimal *pH* and concentration ranges for experiments. Furthermore, introducing relevant inhibitors once CM was detected would have permitted valuable confirmation of the CM components deduced. In conclusion, this study shows the value of combining BBB permeability studies under a range of *pH* and concentration conditions, to improve the accuracy of derived numerical data, and to reveal underlying physiological mechanisms and kinetics of carrier-mediated transport.

Acknowledgement

We are grateful to Prof. Toyofumi Suzuki of Nihon University for providing a table of values corresponding to the plots in Figures 1 and 2 of Suzuki *et al*. (2010a).

Appendix A. *in vitro* flat monolayer permeability model

The description of the *in vitro* cell permeability biophysical analysis is first presented (Yusof *et al.,* 2014; Avdeef *et al.,* 2015), since it is the basis of the capillary *in vivo* permeability data analysis. The *in vitro* apparent endothelial permeability, P_{app}, may be deconvolved into its four underlying components: P_{ABL}, P_{filter}, P_C, and P_{para} (aqueous boundary layer, filter, transendothelial cell membrane, and paracellular, respectively – cf., Abbreviations),

$$\frac{1}{P_{app}} = \frac{1}{P_{ABL}} + \frac{1}{P_f} + \frac{1}{P_C + P_{para}} \tag{A.1}$$

The planar monolayer model is illustrated in Figure 1 (dash-dot-dot curve above ❷ and solid curve below ❷) in the logarithmic form of Eq. (A.1). The capillary flow model is indicated by the thick solid curve in the figure. The other curves are identified and the figure caption and are discussed below. (The filter contribution is not indicated in Fig. 1 for the planar model.)

A.1. Transcellular permeability

For a monoprotic ionizable molecule, the transcellular permeability, P_C, describes the neutral-species permeability (*pH*-partition hypothesis) and is defined by

$$P_C = \frac{P_0}{10^{\pm(pH-pK_a)}+1} \tag{A.2}$$

where the '+' in '±' is used for acids and the '-' is used for bases. For a two-pK_a ampholyte, the denominator term becomes $10^{+pKa1-pH} + 10^{-pKa2+pH} + 1$, where $pK_{a1} < pK_{a2}$. The dashed curve in Figure 1 indicates the hyperbolic log P_C-*pH* profile. The intrinsic permeability, P_0, is indicated at the top of the curve, at the *pH* where the molecule is fully uncharged. The log ($P_C + P_{para}$) vs. *pH* curve is expected to be *sigmoidal* in shape (dashed curve above ❷ and solid curve below ❷ for the planar model). Its minimum possible value is the paracellular permeability. In a purely passive diffusion (PD) process, the transcellular permeability denotes non-saturable lipoidal permeability of the apical, basolateral, and cytosolic-organelle membranes. But saturable carrier-mediated (CM) processes may exist in parallel with the non-saturable PD processes.

A.2. Paracellular permeability

In Eq. (A.1), the dual-pore population paracellular equation (Avdeef and Tam, 2010) is defined as

$$P_{para} = \frac{\varepsilon}{\delta} \cdot D_{aq} \cdot F(r_{HYD}/R) \cdot E(\Delta\varphi) + \left(\frac{\varepsilon}{\delta}\right)_2 \cdot D_{aq} \tag{A.3}$$

The paracellular junction porosity divided by the pore pathlength is indicated by ε/δ. The last term in Eq. (A.3) describes the secondary size/charge-nonspecific "free diffusion" pathway contribution. The E(Δφ) term is a function of the potential drop, Δφ, across the electric field created by negatively-charged

residues lining the junction pores. $F(r_{HYD}/R)$ is the Renkin hydrodynamic sieving function (Ho *et al.,* 2000) for cylindrical water channels, defined as a function of the molecular hydrodynamic radius (r_{HYD}) and junction pore radius (R), both usually expressed in Å units. D_{aq} ($cm^2 \cdot s^{-1}$) is the aqueous diffusivity of the solute at 37°C (related to molecular weight (Avdeef, 2012)). Typical values of the paracellular parameters have been tabulated for several *in vitro* cultured cells (Avdeef, 2010, 2011).

A.3. Filter porosity permeability

In Eq. (A.1), P_f is the filter-porosity permeability, defined as

$$P_f = \varepsilon_f D_{aq} / h_f \quad \text{(A.4)}$$

where ε_f is the filter porosity fraction, which for Transwell™ filters comes in values from 0.003 – 0.008 ('clear filters', polyethylene) to 0.13-0.20 ('translucent filters', polycarbonate) (Yusof *et al*., 2014); h_f is the thickness of the filter (10 µm for polycarbonate). For a molecule with molecular weight 300 Da and a polycarbonate filter with 0.135 porosity, the predicted $P_{filter} = 1079 \times 10^{-6}$ cm·s^{-1}. However, if a clear plastic polyethylene filter is used, with porosity 0.005, then $P_{filter} = 40 \times 10^{-6}$ cm·s^{-1}. Hence, clear filters generally are not suitable for *in vitro* measurements of highly-permeable drugs.

A.4. Aqueous Boundary Layer (ABL) Permeability

In ordinary applications of Eq. (A.1), the aqueous boundary layer (ABL) permeability is defined as

$$P_{ABL} = D_{aq} / h_{ABL} \quad \text{(A.5)}$$

where h_{ABL} is the ABL thickness in the *in vitro* cell assay, which can be predicted from the stirring rate or by the pK_a^{flux} method (Avdeef *et al.,* 2005; Yusof *et al.,* 2014). With microtitre plate methods, typical values of h_{ABL} are near 2000 µm in unstirred solutions, and about 200 µm in solutions stirred at 300 RPM (rev·min^{-1}).

Appendix B. *in vivo* capillary flow permeability model

B.1. BUI Method for moderately lipophilic molecules

In carotid artery injection methods (where a drug solution of concentration C_{inj} is quickly injected), permeability can be determined from the percentage of brain uptake index (BUI), calculated as

$$\text{BUI\%} = E/E_{ref} \times 100 \quad \text{(B.1)}$$

where E and E_{ref} are the extraction fractions of drug and reference compound, often [^{14}C]-butanol, with E_{ref} = 0.64 for rat brain (Terasaki *et al.,* 1986). At 15-s post-injection (in the case study examples considered here), the animal is sacrificed; the drug and reference concentrations in the brain are then determined.

The brain uptake rate (flux per g of brain tissue), J may be defined as

$$\begin{aligned} J = & \quad C_{inj} \cdot F_{pf} \cdot E \\ = & \quad C_{inj} \cdot K_{in} \\ = & - C_{cap} \cdot F_{pf} \cdot \ln (1-E) \\ = & \quad C_{cap} \cdot PS \end{aligned} \tag{B.2}$$

where C_{inj} (mM) is the injectate drug concentration, C_{cap} (mM) is the mean capillary drug concentration, F_{pf} is the cerebral blood flow rate, and PS is the permeability-surface product. The injectate concentration (C_{inj}) is usually greater than the capillary (C_{cap}) value, especially when substantial extraction occurs.

B.2. Crone-Renkin equation (CRE)

Related to the BUI is the transfer constant for the initial brain transport (clearance) of the drug, K_{in} (mL·s^{-1}·g^{-1}), which reflects the unidirectional transport at the luminal BBB membrane (not corrected for flow). In the *in situ* brain perfusion method, the transfer constant is often defined operationally as $K_{in} = (Q_{br} / C_{pf}) / T$, where Q_{br} = test compound parenchymal brain concentration (nmol·g^{-1}) (corrected for the vascular volume), C_{pf} = perfusion fluid concentration (nmol·mL^{-1}), T = perfusion time (s). According to the Crone-Renkin equation (CRE),

$$\begin{aligned} K_{in} &= F_{pf} \cdot E \\ &= F_{pf} \left(1 - e^{-\frac{PS}{F_{pf}}} \right) \end{aligned} \tag{B.3}$$

$K_{in}/S = P_{app}$ (solid curve in Fig. 1), whereas PS/S is the flow-corrected P_C (dashed curve above ❷ and solid curve below ❷ in Fig. 1). When permeability is not limited by flow, $PS = K_{in}$. The endothelial luminal permeability, the 'P' in PS, is defined below (Eqs. (B.8) and (B.9)). The rat brain endothelial surface area (per gram of brain tissue), S (cm^2·g^{-1}), is often approximated to be 100 cm^2·g^{-1} (Ohno *et al.,* 1978). From Eqs. (B.2) and (B.3), the relationship between the C_{inj} and C_{cap} may be stated as

$$C_{cap}/C_{inj} = K_{in}/PS = -E/\ln(1-E) \leq 1 \tag{B.4}$$

According to the transposed CRE from Eq. (B.3),

$$PS = - F_{pf} \ln(1 - K_{in}/F_{pf}) \tag{B.5}$$

B.3. Michaelis-Menten equation (MME)

When carrier-mediated transport is evident, the Michaelis-Menten equation (MME) can be used to separate the saturable from the non-saturable (usually passive) components of transport,

$$J = \frac{J_{\max} C}{K_m + C} + k_d C \tag{B.6}$$

where J_{max} (μmol·min^{-1}·g^{-1}), K_m (mM), and k_d (mL·min^{-1}·g^{-1}) represent the maximal transport rate of the

saturable uptake, the half-saturation concentration (Michaelis constant), and the non-saturable uptake first-order rate constant, respectively. It is very important that the fit be weighted, based on reported experimental errors in the flux values. Using unit weights produces a significantly-different set of MM parameters.

B.4. pH-dependent Michaelis-Menten equation (pH-MME)

When a transporter acts with different specificity for the charged and the neutral forms of a drug, the MME may be expanded to the *pH*-dependent form, *pH*-MME, as

$$J = \frac{J_{\max}^{+} f_{+} C}{K_m^{+} + f_{+} C} + \frac{J_{\max}^{0} f_0 C}{K_m^{0} + f_0 C} + k_d^0 f_0 C \qquad \text{(B.7)}$$

The first term addresses the cationic-species CM process, while the second term addresses the neutral-species CM process. The fraction of the compound in the neutral form is denoted as $f_0 = 1/(10^{\pm(pH-pKa)}+1)$ for a monoprotic drug and $f_0 = 1/(10^{+pKa1-pH} + 10^{-pKa2+pH} +1)$ for a two-pK_a ampholyte, where $pK_{a1} < pK_{a2}$. In addition to CM uptake, the contribution from efflux would require further expansions (Bentz *et al.*, 2005), but this was not considered here.

B.5. pH-dependent Crone-Renkin equation for flow correction

If K_{in} (or k_d) of an ionizable drug (with acid $pK_a < 9$ or base $pK_a > 5$) were measured at more than one *pH*, F_{pf} could be determined without the use of a standard flow marker, such as diazepam (Smith, 2003). Eq. (A.1), without the filter contribution, is approximately valid when applied to *in vivo* measurement:

$$\frac{1}{P_{app}} = \frac{1}{F_{pf}/S} + \frac{1}{P_C + P_i + P_{para}} \qquad \text{(B.8)}$$

where

$$P_i = \frac{P_{+}}{(10^{\pm(pK_a - pH)} + 1)} \qquad \text{(B.9)}$$

('-' sign for bases and the '+' sign for acids). The first term in Eq. (B.8) refers to the capillary flow "resistance," while the second term refers to the endothelial cell "resistance," comprising the transcellular (P_C and P_i) and paracellular (P_{para}) contributions. Eq. (B.8) is the "monolayer" approximation to the flow equation described below. The small differences between the exact capillary tubular flow (solid line in Fig. 1) and planar monolayer (dash-dot-dot line in Fig. 1) models are evident near the bend in the curve where the horizontal flow limit (dotted line) and the diagonal transcellular (dashed line) curves intersect, as indicated by pK_a^{flux} in Figure 1. For a monoprotic acid or base, the relationship between the effective luminal permeability, P_{app}, and *pH* can be stated as a sum of three permeability components – (i) neutral species (P_C) curve, (ii) charged species (P_i) curve, as in case of carrier-mediated effects, and (iii) leaked species through paracellular water-filled pores in the tight junctions between endothelial cells (P_{para}).

Normally, paracellular junctions at the BBB are very tight (cf., BBB paracellular parameters in Eq. (A.3) above). For the rodent BBB, the empirical parameters have been estimated as ε/δ = 6.7 ± 4.5 cm^{-1}, R = 4.8 ± 0.4 Å, ε/δ_2 = 0.009 ± 0.017 cm^{-1} (Avdeef, 2012). For example, the predicted BBB paracellular permeability of sucrose is predicted to be $P_{para}^{sucrose}$ = 0.07 x 10^{-6} cm·s^{-1}. In many cases, P_i can be neglected, unless the charged form of the drug is a substrate of a carrier-mediated transport.

In logarithmic form, the second line of Eq. (B.3) may be expanded according to Eq. (B.9) to produce

$$\log K_{in}^{calc}(F_{pf}, P_o, P_i, P_{para}) = \log F_{pf} + \log\left[1 - e^{-\left(\frac{P_o}{(10^{\pm(pH-pK_a)}+1)} + \frac{P_i}{(10^{\pm(pK_a-pH)}+1)} + P_{para}\right)\cdot\frac{S}{F_{pf}}}\right] \quad \text{(B.10)}$$

The above *pH*-CRE flow correction method can be applied to a flow- or near flow-limited ionizable drug (whose pK_a value is known at 37°C (Avdeef and Sun, 2011)). Ideally, K_{in} is measured in at least two different *pH* buffers in the *pH* 5.5 – 8.5 range. At least one point (❶ in Fig. 1) needs to be at a *pH* where the molecule is nearly uncharged and P_C is high (near or exceeding the flow limit), and one point (❷ in Fig. 1) needs to be at the *pH* where the molecule is partly charged and P_C is lower (sufficiently below the flow limit). If ionic-species transport exceeding paracellular permeability is suspected (*e.g.*, by a bend in the log P_{app}-*pH* curve in Fig. 1 near *pH* 5.5), then at least a third K_{in} needs to be measured (❸ in Fig. 1). The computational method does not require an external flow calibrant like diazepam. Moreover, the drug chosen for the *pH*-CRE analysis can also serve as a suitable substitute for diazepam in the traditional CRE method, since the value of F_{pf} is also determined by the *pH*-CRE analysis. Perhaps the most important use of the *pH*-CRE is to obtain a relevant *in vivo* dataset for validating *in vitro* assays, which is challenging to do for lipophilic drugs by traditional techniques.

References

Adson, A., Burton, P.S., Raub, T.J., Barsuhn, C.L., Audus, K.L., Ho, N.F.H., 1995. Passive diffusion of weak organic electrolytes across Caco-2 cell monolayers: uncoupling the contributions of hydrodynamic, transcellular, and paracellular barriers. J. Pharm. Sci. 84, 1197-1204.

Alsenz, J., Haenel, E., 2003. Development of a 7-day, 96-well Caco-2 permeability assay with high-throughput direct UV compound analysis. Pharm. Res. 20, 1961-1969.

Agarwal, S., Jain, R., Pal, D., Mitra, A.K., 2007. Functional characterization of peptide transporters in MDCKII-MDR1 cell line as a model for oral absorption studies. Int. J. Pharm. 332, 147-152.

Avdeef, A., Artursson, P., Neuhoff, S., Lazarova, L., Gräsjö, J., Tavelin, S., 2005. Caco-2 permeability of weakly basic drugs predicted with the Double-Sink PAMPA pK_a^{flux} method. Eur. J. Pharm. Sci. 24, 333-349.

Avdeef, A., Tam, K.Y., 2010. How well can the Caco-2/MDCK models predict effective human jejunal permeability? J. Med. Chem. 53, 3566-3584.

Avdeef, A., 2010. Leakiness and size exclusion of paracellular channels in cultured epithelial cell monolayers – interlaboratory comparison. Pharm. Res. 27, 480-489.

Avdeef, A., 2011. How well can *in vitro* barrier capillary endothelial cell models predict *in vivo* blood-brain barrier permeability? Eur. J. Pharm. Sci. 43, 109-124.

Avdeef, A., Sun, N., 2011. A new *in situ* brain perfusion flow correction method for lipophilic drugs based on the *pH*-dependent Crone-Renkin equation. Pharm. Res. 28, 517-530.

Avdeef, A., 2012. Absorption and Drug Development Second Edition. Wiley-Interscience, Hoboken, NJ.

Avdeef, A., Deli, M.A., Neuhaus, W., 2015. In-vitro assays for assessing BBB permeability: artificial membrane and cell culture models. In: Di L, Kerns EH (eds.). Blood-Brain Barrier in Drug Discovery: Optimizing Brain Exposure of CNS Drugs and Minimizing Brain Side Effects. Wiley-Interscience. Hoboken, NJ., pp. 188-237.

Bentz, J., Tran, T.T., Polli, J.W., Ayrton, A., Ellens, H., 2005. The steady-state Michaelis-Menten analysis of P-glycoprotein mediated transport through a confluent cell monolayer cannot predict the correct Michaelis constant K_m. Pharm Res. 22, 1667-1677.

Berginc, K., Zakelj, S., Levstik, L., Ursic, D., Kristl, A., 2007. Fluorescein transport properties across artificial lipid membranes, Caco-2 cell monolayers and rat jejunum. Eur. J. Pharm. Biopharm. 66, 281-285.

Bhardwaj, R.K., Herrera-Ruiz, D., Sinko, P., Gudmundsson, O.S., Knipp, G., 2005. Delineation of human peptide transporter 1 (hPepT1)-mediated uptake and transport of substrates with varying transporter affinities utilizing stably transfected hPepT1/Madin-Darby Canine Kidney Clones and Caco-2 cells. J. Pharmacol. Exp. Ther. 314, 1093-1100.

Collett, A., Walker, D., Sims, E., He, Y.-L., Speers, P., Ayrton, J., Rowland, M., Warhurst, G., 1997. Influence of morphmetric factors on quantitation of paracellular permeability of intestinal epithelia *in vitro*. Pharm. Res. 14, 767-773.

Desesso, J.M., Williams, A.L., 2008. Contrasting the gastrointestinal tracts of mammals: factors that influence absorption. Annual Rep. Med. Chem. 43, 353-371.

Greenwood, J., Hazell, A.S., Luthert, P.J., 1989. The effect of a low *pH* saline perfusate upon the integrity of the energy-depleted rat blood-brain barrier. J. Cereb. Blood Flow Metab. 9, 234-242.

Ho, N.F.H., Raub, T.J., Burton, P.S., Barsuhn, C.L., Adson, A., Audus, K.L., Borchardt, R.T., 2000. Quantitative approaches to delineate passive transport mechanisms in cell culture monolayers. In: Amidon, G.L.; Lee, P.I.; Topp, E.M. (Eds.) Transport Processes in Pharmaceutical Systems. Marcel Dekker: New York, pp. 219-317.

Högerle, M.L.,Winne, D., 1983. Drug absorption by the rat jejunum perfused *in situ*. Dissociation from the *pH*-partition theory and the role of microclimate-*pH* and unstirred layer. Naunyn-Schmiedeberg's Arch. Pharmacol. 322, 249-255.

Kanaan, M., Daali, Y., Dayer, P., Desmeules, J., 2008. Lack of interaction of the NMDA receptor antagonists dextromethorphan and dextrorphan with P-glycoprotein. Curr. Drug Metab. 9, 144-151.

Kansy, M., Fischer, H., Kratzat, K., Senner, F., Wagner, B., Parrilla, I., 2001. High-throughput artificial membrane permeability studies in early lead discovery and development. In: Testa, B.; van de Waterbeemd, H.; Folkers, G.; Guy, R. (Eds.). Pharmacokinetic Optimization in Drug Research, Verlag Helvetica Chimica Acta: Zürich and Wiley - VCH: Weinheim, pp. 447-464.

Kararli, T.T., 1995. Comparison of the gastrointestinal anatomy, physiology, and biochemistry of humans and commonly used laboratory animals. Biopharm. Drug Disp. 16, 351–380.

Kaufman, J.J., Semo, N.M., Koski, W.S., 1975. Microelectrometric titration measurement of the pK_a`s and partition and drug distribution coefficients of narcotics and narcotic antagonists and their *pH* and temperature dependence. J. Med. Chem. 18, 647-655.

Korjamo, T., Heikkinen, A.T., Waltari, P., Mönkkönen, J., 2008. The asymmetry of the unstirred water layer in permeability experiments. Pharm. Res. 25, 1714-1722.

Laitinen, L., Kangas, H., Kaukonen, A.M., Hakala, K., Kotiaho, T., Kostianen, R., Hirvonen, J., 2003. N-in-one permeability studies of heterogeneous sets of compounds across Caco-2 cell monolayers. Pharm. Res. 20, 187-197.

Lee, K.-J., Johnson, N., Castelo, J., Sinko, P.J., Grass, G., Holme, K., Lee, Y.-H., 2005. Effect of experimental *pH* on the *in vitro* permeability in intact rabbit intestines and Caco-2 monolayer. Eur. J. Pharm. Sci. 25, 193-200.

Neuhoff, S., Ungell, A.-L., Zamora, I., Artursson, P., 2003. *pH*-dependent bidirectional transport of weakly basic drugs across Caco-2 monolayers: implications for drug-drug interactions. Pharm. Res. 20, 1141-1148.

Neuhoff, S., Ungell, A.-L., Zamora, I., Artursson, P., 2005. *pH*-dependent passive and active transport of acidic drugs across Caco-2 cell monolayers. Eur. J. Pharm. Sci. 25, 211-220.

Ohno, K., Pettigrew, K.D., Rapoport, S.I., 1978. Lower limits of cerebrovascular permeability to

nonelectrolytes in the conscious rat. Am. J. Physiol. 235, H299-H307.

Okura, T., Hattori, A., Takano, Y., Sato, T., Hammarlund-Udenaes, M., Terasaki, T., Deguchi, Y., 2008. Involvement of the pyrilamine transporter, a putative organic cation transporter, in blood-brain barrier transport of oxycodone. Drug Metab. Dispos. 36, 2005-2013.

Pade, V., Stavchansky, S., 1985. Estimation of the relative contribution of the transcellular and paracellular pathway to the transport of passively absorbed drugs in the Caco-2 cell culture model. Pharm. Res. 1997, 14, 1210-1215.

Palm, K., Luthman, K., Ros, J., Grasjo, J., Artursson, P., 1999. Effect of molecular charge on intestinal epithelial drug transport: *pH*-dependent transport of cationic drugs. J. Phamacol. Exp. Ther. 291, 435-443.

Pardridge, W.M., Fierer, G., 1985. Blood-brain barrier transport of butanol and water relative to N-isopropyl-p-iodoamphetamine as the internal reference. J Cereb Blood Flow Metab. 5, 275-281.

Raeissi, S.D., Li, J., Hidalgo, I.J., 1999. The role of an alpha-amino group on H+-dependent transepithelial transport of cephalosporins in Caco-2 cells. J. Pharm. Pharmacol. 51, 35-40.

Smith, Q.R., 2003. A review of blood-brain barrier transport techniques. Methods Mol. Med. 89, 193-208.

Sun, N., Avdeef, A., 2011. Biorelevant pK_a (37 ^{o}C) predicted from the 2D structure of the molecule and its pK_a at 25 ^{o}C. J. Pharm. Biomed. Anal. 56, 173-182.

Suzuki, T., Moriki, Y., Goto, H., Tomono, K., Hanano, M., Watanabe, J., 2002a. Investigation on the influx transport mechanism of pentazocine at the blood-brain barrier in rats using the carotid injection technique. Biol. Pharm. Bull. 25, 1351-1355.

Suzuki, T., Oshimi, M., Tomono, K., Hanano, M., Watanabe, J., 2002b. Investigation of transport mechanism of pentazocine across the blood-brain barrier using the *in situ* rat brain perfusion. J. Pharm. Sci. 91, 2346-2353.

Suzuki, T., Ohmuro, A., Miyata, M., Furuishi, T., Hidaka, S., Kugawa, F., Fukami, T., Tomono, K., 2010a. Involvement of an influx transporter in the blood-brain barrier transport of naloxone. Biopharm. Drug Dispos. 31, 243-252.

Suzuki T, Miyata M, Zaima C, Furuishi T, Fukami T, Kugawa F, Tomono K., 2010b. Blood-brain barrier transport of naloxone does not involve P-glycoprotein-mediated efflux. J. Pharm. Sci. 99, 413–421.

Suzuki, T., Aoyama, T., Suzuki, N., Kobayashi, M., Fukami, T., Matsumoto, Y., Tomono, K., 2016. Involvement of a proton-coupled organic cation antiporter in the blood–brain barrier transport of amantadine. Biopharm. Drug Dispos. 37, 323–335.

Takanaga, H., Tamai, I., Tsuji, A., 1994. *pH*-Dependent and carrier-mediated transport of salicylic acid across Caco-2 cells. J. Pharm. Pharmacol. 46, 567-570.

Takasato, Y., Rapoport, S.I., Smith, Q.R., 1984. An *in situ* brain perfusion technique to study cerebrovascular transport in the rat. Am. J. Physiol. 247, H484-H493.

Terasaki, T., Pardridge, W. M., Denson, D. D., 1986. Differential effect of plasma protein binding of bupivacaine on its *in vivo* transfer into the brain and salivary gland of rats. J. Pharmacol. Exp. Ther., 239, 724-729.

Thomson, A.B.R., Dietschy, J.M., 1977. Derivation of the equations that describe the effects of unstirred water layers on the kinetic parameters of active transport processes in the intestine. J. Theor. Biol. 64, 277-294.

Tsinman, O., Tsinman, K., Sun, N., Avdeef, A., 2011. Physicochemical selectivity of the BBB microenvironment governing passive diffusion – matching with a porcine brain lipid extract artificial membrane permeability model. Pharm. Res. 28, 337-363.

Tsuji, A., Takanaga, H., Tamai, I., Terasaki, T., 1994. Transcellular transport of benzoic acid across Caco-2 cells by a *pH*-dependent and carrier-mediated transport mechanism. Pharm. Res. 11, 30-37.

Wilson, J.P., 1967. Surface area of the small intestine in man. Gut 8, 618-621.

Wilson, T.D., 1984. Pentazocine. Analytical Profiles of Drug Substances 13, 361-416.

Yamashita, S., Furubayashi, T., Kataoka, M., Sakane, T., Sezaki, H., Tokuda, H., 2000. Optimized conditions for prediction of intestinal drug permeability using Caco-2 cells. Eur. J. Pharm. Sci. 10, 109-204.

Yokogawa, K., Nakashima, E., Ishizaki, J., Maeda, H., Nagano, T., Ichimaru, F., 1990. Relationships in the structure-tissue distribution of basic drugs in the rabbit. Pharm. Res. 7, 691-696.

Yu, L., Zeng, S., 2007. Transport characteristics of zolmitriptan in a human intestinal epithelial cell line Caco-2. J. Pharm. Pharmacol. 59, 655-660.

Yusof, S.R., Avdeef, A., Abbott, N.J., 2014. *In vitro* porcine blood-brain barrier model for permeability studies: pCEL-X software pK_a^{flux} method for aqueous boundary layer correction and detailed data analysis. Eur. J. Pharm. Sci. 65, 98-111.

Figure Captions

Fig. 1. Characteristics of the capillary- and planar-based equations for a hypothetical moderately lipophilic base molecule: pK_a = 9.0, P_0 = 10^{-2} cm·s^{-1}, P_+ = 10^{-5} cm·s^{-1}, S = 100 cm^2·g^{-1}, F_{pf} = 0.04 mL·g^{-1}·s^{-1} (log (F_{pf}/S) = -3.40). For comparison of the two hydrodynamic models, the calculation assumed log P_{ABL} = -3.40 (same as log (F_{pf}/S)). The thick solid curve represents log P_{app} (=log $(K_{in}/S$ = log $(k_d/S))$); see text . The dash-dot-dot curve denotes where the monolayer model departs from the capillary model. The dashed curve represents the transcellular membrane permeability due to the uncharged species, according to the *pH*-partition hypothesis. It also may include the contribution due to a CM process affecting the neutral species. The dash-dot curve is due to paracellular permeability. The horizontal dotted line indicates the permeability limit due to the hydrodynamic effects (flow limit or ABL). The P_{app} curves have a slope of 1 before the central bend and a slope of zero after the bend. The *pH* in the middle of the central bend is called pK_a^{flux}, where 50% of the permeation is due to transcellular membrane permeability and 50% due to the apparent/effective permeability as a consequence of the hydrodynamic effect. The intrinsic permeability can be estimated for ionizable flow-limited molecules (*i.e.*, $P_0 >> F_{pf}/S$) from log P_0 = log (F_{pf}/S) + | $pK_a - pK_a^{flux}$ |. The dynamic range window (DRW) defines where permeability can be directly measured. The DRW ceiling is the flow/ABL limit; its floor is the paracellular limit.

Fig. 2. *pH*-dependent Crone-Renkin equation analysis of rat *in situ* brain perfusion (ISBP) data of oxycodone. The lower (blue) solid curve is the best fit to the data measured in the presence of 1 mM pyrilamine (as inhibitor). The upper (red) curve represents the assay results in the absence of inhibitor. The uptake was mildly flow limited for both the with- and without-inhibitor data sets, with nearly the same F_{pf} values of 0.020 (without inhibitor) and 0.016 (with 1 mM pyrilamine inhibitor) mL·s^{-1}·g^{-1}.

Fig. 3. *pH*-dependent Crone-Renkin equation analyses of (a) the *in vivo* rat carotid artery injection (BUI) data, and (b) the *in situ* brain perfusion (ISBP) data of pentazocine. The lower (blue) solid curve is the best fit to the data measured at/near saturating levels of injectate (12-40 mM). The upper (red) solid curve represents the assay results at the low injectate concentration, ≤ 0.1 mM, where both influx and efflux transport mechanisms may be operative (Suzuki *et al*., 2002a, 2002b). Only the low-concentration set indicates a flow limit, with the F_{pf} value of 0.0082 (BUI) and 0.0091 mL·s^{-1}·g^{-1} (ISBP). The dashed (neutral) and dash-dot (cation) curves result from the deconvolution of the best-fit solid curves based on the measured points.

Fig. 4. (a, b) The original BUI pentazocine uptake curves (Suzuki *et al.,* 2002a), flux vs. mean capillary concentration (*J* vs. C_{cap}), were re-calculated using the experimental F_{pf} values determined by the *pH*-dependent Crone-Renkin equation analysis. The ISBP data (Suzuki *et al.,* 2002b) were similarly treated (see text). The Michaelis-Menten parameters are summarized in Table 3. The unfilled circles are the reported mean capillary concentrations. The filled-circle data are those calculated after adjustment corrections for the flow determined by the *pH*-CRE method.

Fig. 5. *pH*-dependent Crone-Renkin equation analyses of the *in vivo* rat carotid artery injection (BUI) data of naloxone. The lower (blue) solid curve is the best fit to the data measured under saturating levels of injectate (10 mM). The upper (red) solid curve represents the assay results at the low injectate concentration, 0.1 µM, where the uptake transport mechanism (Suzuki *et al*., 2010a) is evident. Both sets of data indicate the same flow limit, with the F_{pf} value of 0.0055 mL·s^{-1}·g^{-1}. The dashed (neutral) and dash-

dot (cation) curves result from the deconvolution of the best-fit solid curves based on the measured points.

Fig. 6. The original naloxone BUI uptake curve (Fig. 1 in Suzuki *et al.,* 2010a), flux vs. mean capillary concentration (J vs. C_{cap}), was re-calculated using the experimental F_{pf} values determined by the *pH*-CRE analysis. The unfilled circles are the data reported by Suzuki *et al*., prior to flow corrections.

Fig. 7. (a) Naloxone BUI Michaelis-Menten analysis as a function of *pH*, based on two concentration points at each *pH* (cf., Fig. 6), with k_d values provided as fixed parameters (taken from the dash-dot-dot curve in Fig. 5). (b) Percentage of carrier-mediated transport contribution as a function of *pH*. At *pH* 8.5, where the naloxone ampholyte is uncharged, CM contribution to transport is 58%. Passive permeability only accounts for 42% of the transport.

Table 1

Physical Properties of the Compounds Studied [a]

Compound	MW	$pK_{a1}^{37°C}$	$pK_{a2}^{37°C}$	Type [b]	log *P* octanol-water	log P_0 PAMPA-BBB [c]	log P_0 Caco-2 [d]	r_{HYD} (Å) [e]	D_{aq} (10^{-6} $cm^2.s^{-1}$) [f]
Naloxone	327.37	7.82	9.25	BA	1.81	-3.49	-3.63	4.48	7.19
Oxycodone	315.36	8.73		B	0.7	-3.92	-3.70	4.42	7.31
Pentazocine	285.42	9.16	9.96	BA	3.31	-1.88	-2.29	4.48	7.65

[a] Intrinsic permeability, hydrodynamic radius, and aqueous diffusivity were calculated using *p*CEL-X (*in-ADME* Research).

[b] B = base, BA = ampholyte. pK_a values from Wiki-pK_a database (www.in-adme.com/tools.html).

[c] Intrinsic PAMPA-BBB permeability.

[d] Intrinsic Caco-2 permeability.

[e] Hydrodynamic radius of molecule.

[f] Aqueous diffusivity.

Table 2

Rat blood-brain barrier apparent permeability data used in the study [a]

pH	log $P_{app}^{in\ vivo}$ (cm.s^{-1})	SD	C_{inj} (mM)	C_{cap} (mM)	J (µmol.min^{-1}.g^{-1})	SD
Naloxone - carotid artery injections (BUI method) [b]						
5.5	-4.55	0.02	1E-04	7.1E-05	1.7E-05	6.5E-07
6.0	-4.54	0.03	1E-04	7.1E-05	1.7E-05	1.1E-06
6.5	-4.51	0.03	1E-04	6.8E-05	1.8E-05	1.1E-06
7.0	-4.45	0.02	1E-04	6.2E-05	2.1E-05	1.1E-06
7.4	-4.36	0.01	1E-04	5.1E-05	2.6E-05	3.6E-07
8.0	-4.30	0.02	1E-04	3.9E-05	3.0E-05	1.4E-06
8.5	-4.29	0.01	1E-04	3.4E-05	3.1E-05	7.7E-07
5.5	-4.69	0.07	10	8.00	1.22	0.19
6.0	-4.69	0.07	10	7.99	1.23	0.19
6.5	-4.64	0.03	10	7.75	1.37	0.11
7.0	-4.56	0.04	10	7.18	1.67	0.17
7.4	-4.50	0.03	10	6.75	1.88	0.12
7.4	-4.34	0.03	5.9E-04	2.7E-04	1.6E-04	1.3E-05
	-4.39	0.01	1.2E-03	6.4E-04	2.8E-04	4.2E-06
	-4.37	0.02	1.0E-02	5.1E-03	2.6E-03	1.4E-04
	-4.32	0.03	0.10	0.043	0.029	0.002
	-4.43	0.02	0.57	0.35	0.13	0.01
	-4.40	0.02	1.02	0.57	0.24	0.01
	-4.43	0.02	2.29	1.36	0.51	0.02
	-4.45	0.01	5.00	3.09	1.07	0.04
	-4.50	0.03	10.00	6.75	1.88	0.12
	-4.56	0.02	15.93	11.43	2.66	0.12
Pentazocine - carotid artery injections (BUI method) [c]						
5.5	-4.72	0.03	0.1	0.094	0.011	0.001
6.5	-4.43	0.06	0.1	0.087	0.022	0.003
7.4	-4.10	0.03	0.1	0.072	0.047	0.003
5.5	-4.47	0.15	1	0.78	0.20	0.07
	-4.73	0.12	3	2.65	0.33	0.09
	-4.73	0.06	6	5.29	0.67	0.10
	-4.88	0.04	12	11.01	0.94	0.09
	-4.93	0.04	18	16.68	1.26	0.12
	-4.95	0.02	30	27.89	2.03	0.09
	-5.02	0.02	40	37.61	2.31	0.12
7.4	-4.14	0.03	3	1.20	1.32	0.08
	-4.20	0.03	6	3.19	2.25	0.15
	-4.31	0.05	12	7.90	3.51	0.40
	-4.39	0.02	18	13.04	4.38	0.25

	-4.60	0.03	30	25.15	4.50	0.29
	-4.65	0.02	40	34.25	5.37	0.28
Pentazocine - in situ brain perfusion (ISBP method) [d]						
5.5	-4.43	0.08	$2x10^{-5}$			
	-4.94	0.01	12			
6.5	-4.18	0.06	$2x10^{-5}$			
7.4	-4.04	0.04	$2x10^{-5}$			
	-4.47	0.01	12			
	-4.64	0.04	30			
5.5			$2x10^{-5}$		$5.78x10^{-6}$	$4.2x10^{-7}$
			3		0.45	0.02
			6		0.47	0.03
			12		0.90	0.02
7.4			0.01		0.03	999 [f]
			1		1.32	999 [f]
			3		1.50	0.03
			6		2.01	0.07
			12		3.08	0.06
			18		3.15	0.21
			30		4.77	0.34
Oxycodone - *in situ* brain perfusion method (+0 mM pyrilamine) [e]						
7.4	-4.43	0.06				
8.4	-3.81	0.03				
Oxycodone - *in situ* brain perfusion method (+1 mM pyrilamine) [e]						
7.4	-4.77	0.03				
8.4	-4.06	0.03				

[a] $P_{app}^{in\ vivo}$ is the apparent luminal permeability (cf., Eq. (B.7)). C_{inj} is the injectate concentration of drug. C_{cap} is the mean capillary concentration of drug (cf., Eq. (B.2)). J is the brain uptake rate (cf., Eq. (B.2)).

[b] Suzuki *et al.*, 2010.

[c] Suzuki *et al.*, 2002a.

[d] Suzuki *et al.*, 2002b.

[e] Okura *et al.*, 2008.

[f] Point zero-weighted in the refinement.

Table 3

Pentazocine Michaelis-Menten analysis of brain uptake in rodent [a]

Method	*pH*	J_{max} (µmol· min^{-1}·g^{-1})	K_m (mM)	J_{max} / K_m (mL·min^{-1}·g^{-1})	k_d (mL·min^{-1}·g^{-1})	GOF	n	C_{cap} or C_{pf} (mM)	CM%	NS%	Comment
BUI	5.5	0.5 ± 0.2	2.4 ± 2.5	0.21	0.05 ± 0.01	0.8	7	0.8 - 38	80	20	Fig. 4a
	7.4	4.6 ± 0.8	3.3 ± 0.8	1.42	0.03 ± 0.02	0.9	6	1.2 - 34	98	2	Fig. 4b
	5.5	4.7 ± 0.8	40 ± 11	0.12	0.0013 (not varied)	1.1	7	0.8 - 38	99	1	k_d calc from log P_0 -3.08
	7.4	2.7 ± 0.2	1.4 ± 0.3	1.94	0.0983 (not varied)	1.8	6	1.2 - 34	95	5	k_d calc from log P_0 -3.08
ISBP	5.5	0.3 ± 0.1	1.4 ± 0.3	0.25	0.05 ± 0.01	2.9	4	$2x10^{-5}$- 12	84	16	Fig. 4c
	7.4	1.4 ± 0.1	0.49 ± 0.02	2.79	0.13 ± 0.01	2.9	7	0.01 - 30	95	5	Fig. 4d
	5.5	1.6 ± 0.2	11 ± 2	0.15	0.0013 (not varied)	4.4	3	3 - 12	99	1	k_d calc from log P_0 -3.08
	7.4	1.7 ± 0.1	0.8 ± 0.1	2.23	0.0983 (not varied)	3.9	6	1 - 30	96	4	k_d calc from log P_0 -3.08
BUI	5.5	0.9 ± 0.4	7.6 ± 3.5	0.12	0.04 ± 0.01		7	0.9 - 39	75	25	Suzuki et al. 2002a
	7.4	3.6 ± 1.2	3.7 ± 1.7	0.97	0.06 ± 0.04		8	0.6 - 37	94	6	Suzuki et al. 2002a
ISBP	5.5	0.4 ± 0.3	1.8 ± 1.4	0.21	0.04 ± 0.03		4	$2x10^{-5}$- 12	85	15	Suzuki et al. 2002b
	7.4	1.6 ± 0.3	2.9 ± 0.5	0.56	0.09 ± 0.02		7	0.01 - 30	86	14	Suzuki et al. 2002b

[a] BUI = brain uptake index (carotid artery injection), ISBP = in situ brain perfusion; J_{max}/K_m carrier contribution to flux, in limit of zero concentration

CM% = percentage of transport due to saturable carrier-mediated process in the limit of zero concentration

NS% = percentage due to nonsaturable (passive diffusion) process in the limit of zero concentration

C_{cap} = mean capillary concentration of drug (in BUI method), C_{pf} = drug concentration in the perfusion solution (in ISBP method).

GOF - goodness-of-fit (cf., Sec. 2.3); n = number of measurements used in the weighted nonlinear regression analysis.

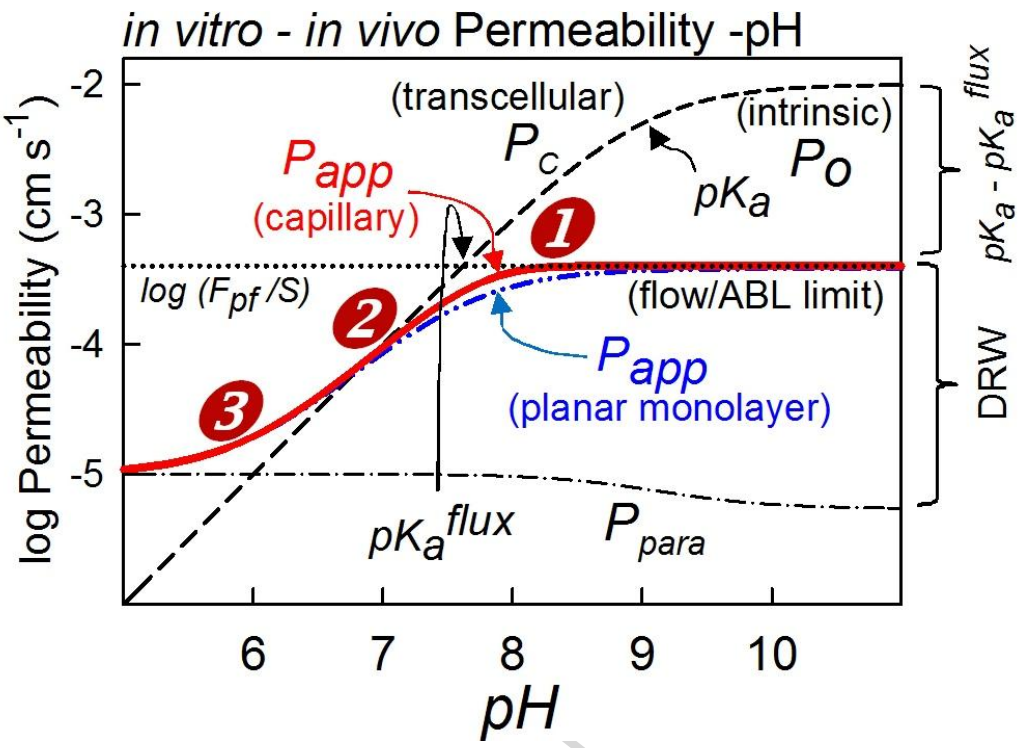

Figure 1

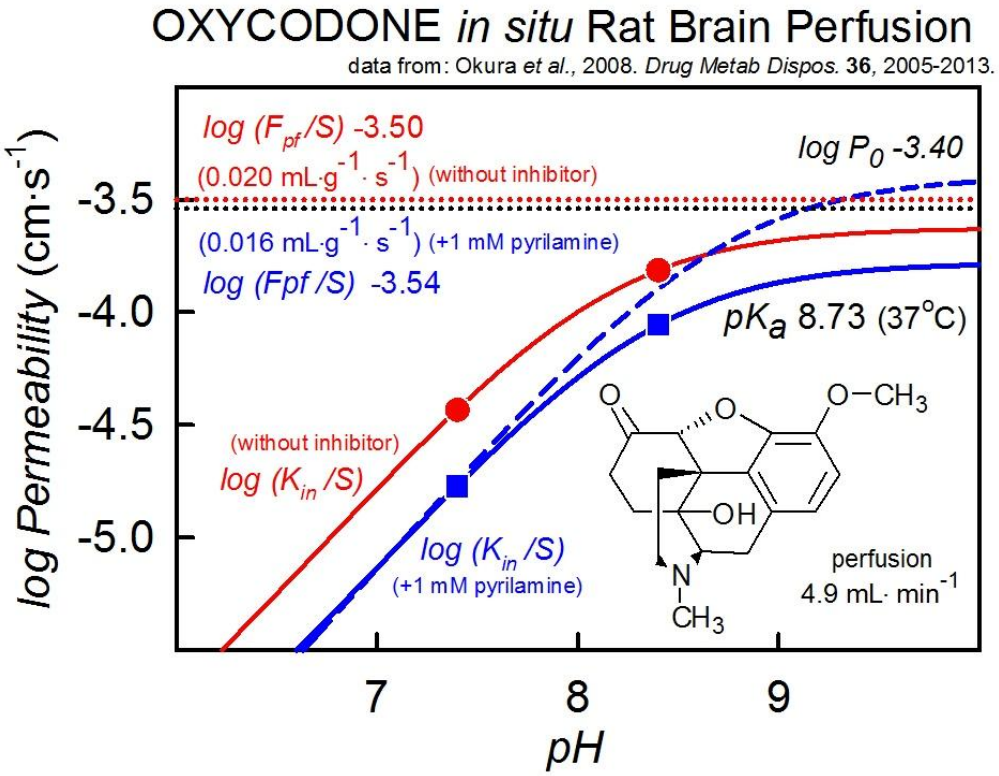

Figure 2

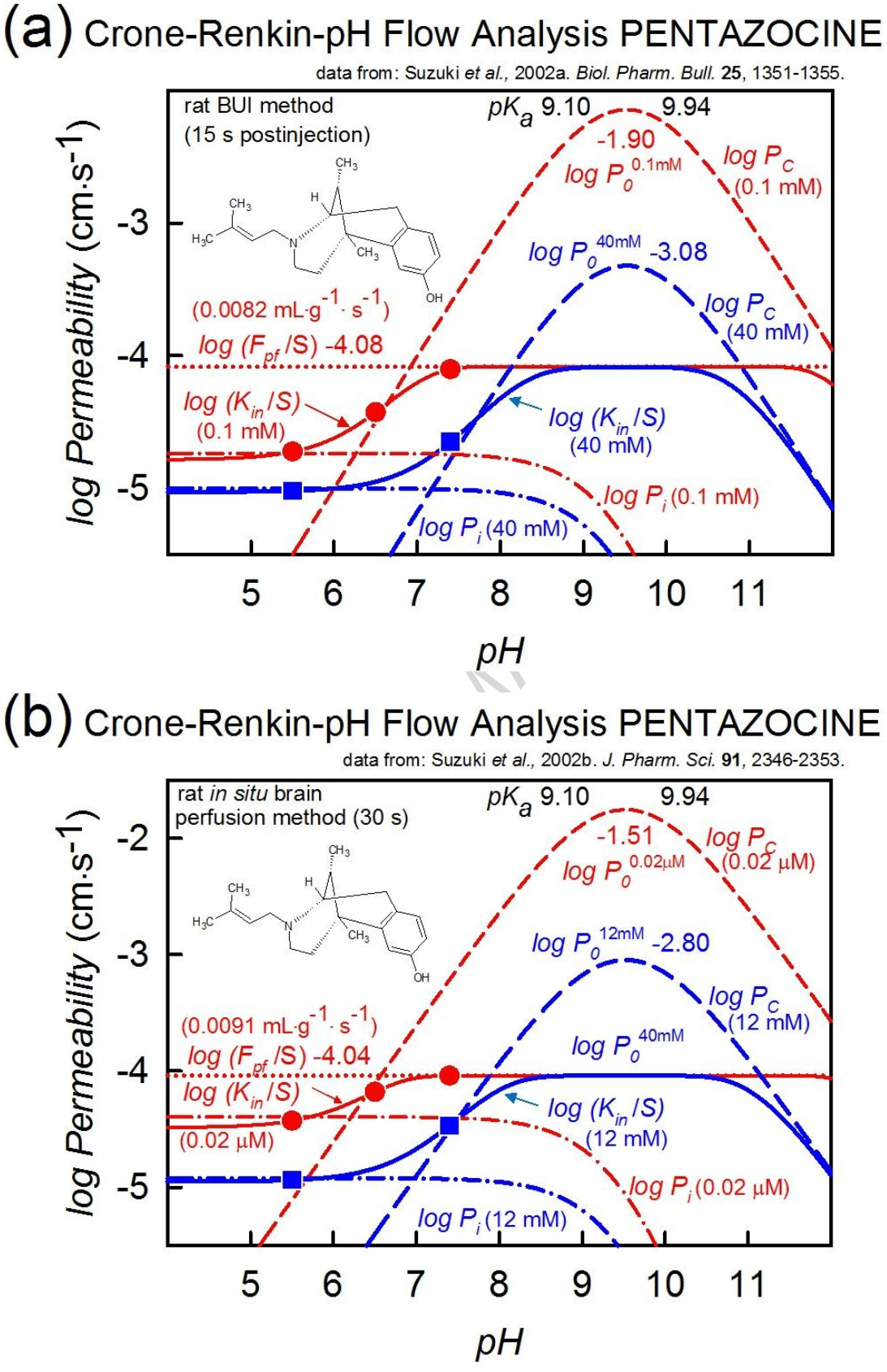

Figure 3

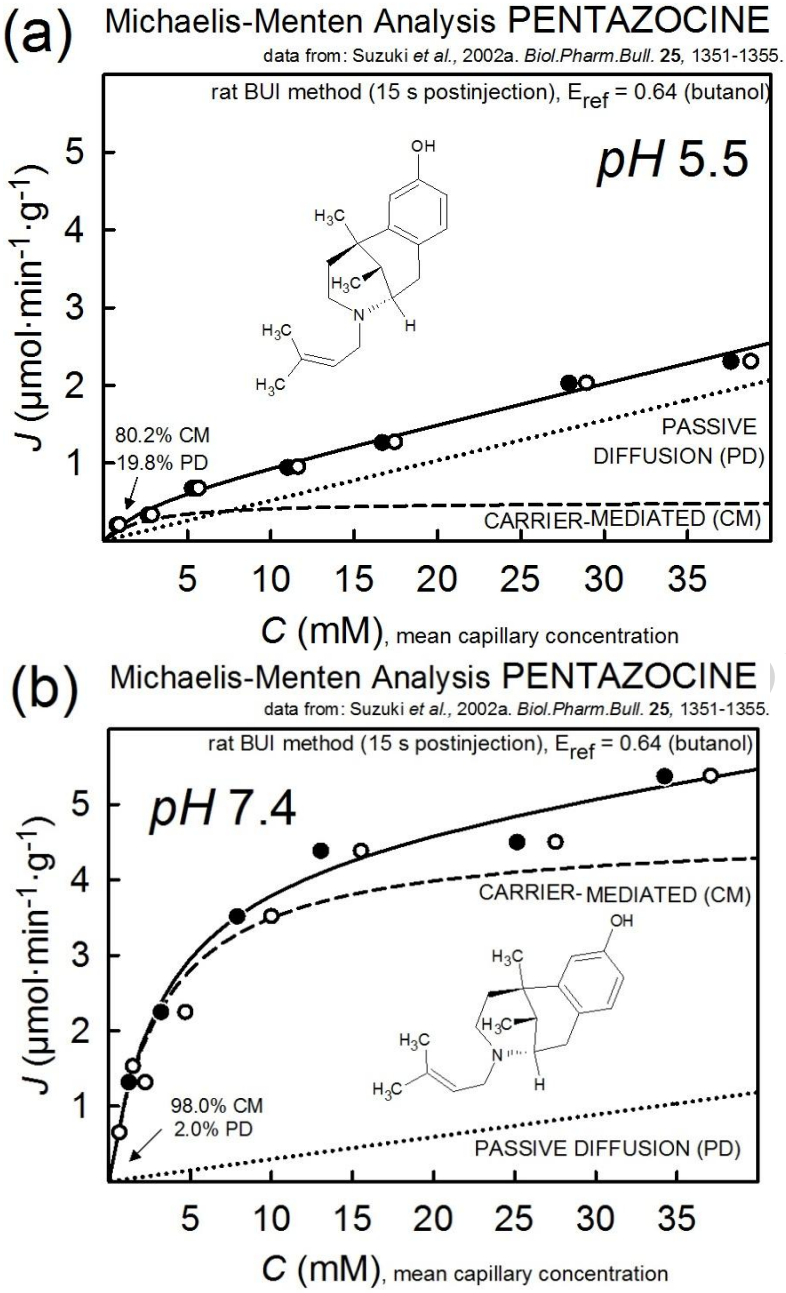

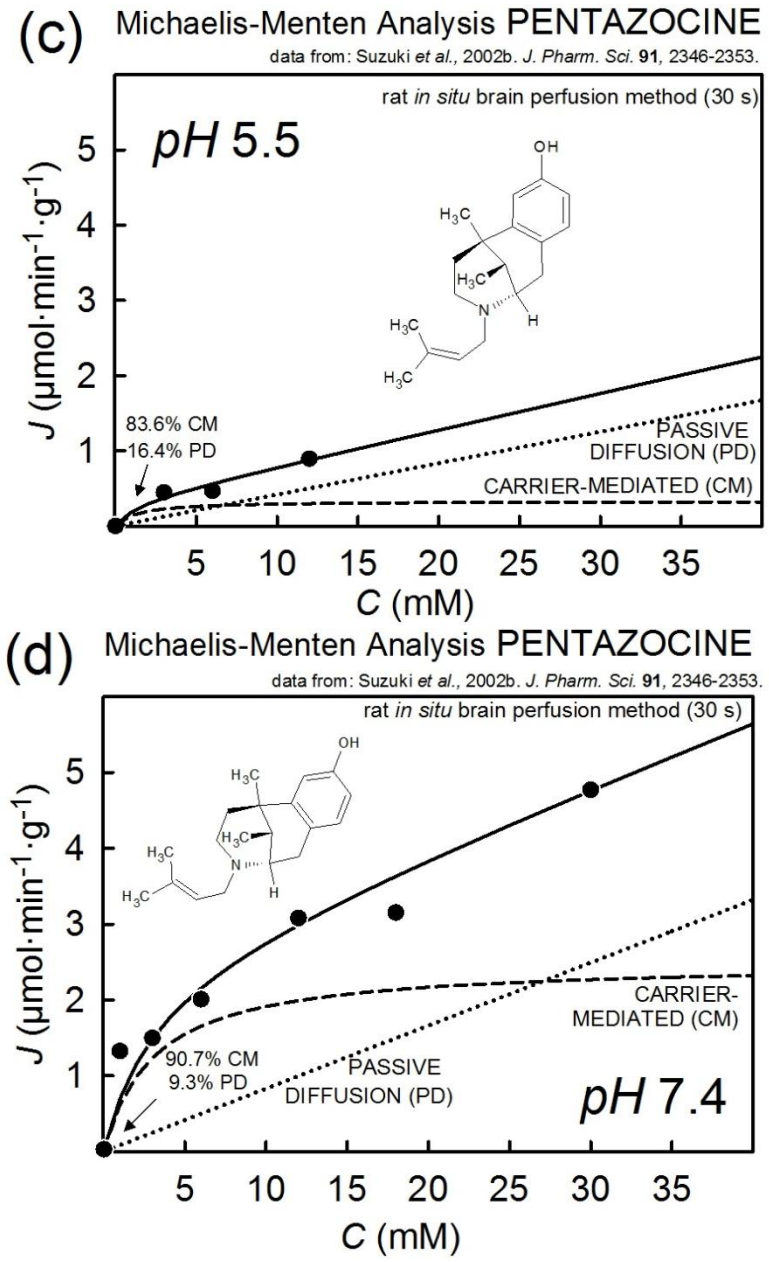

Figure 4

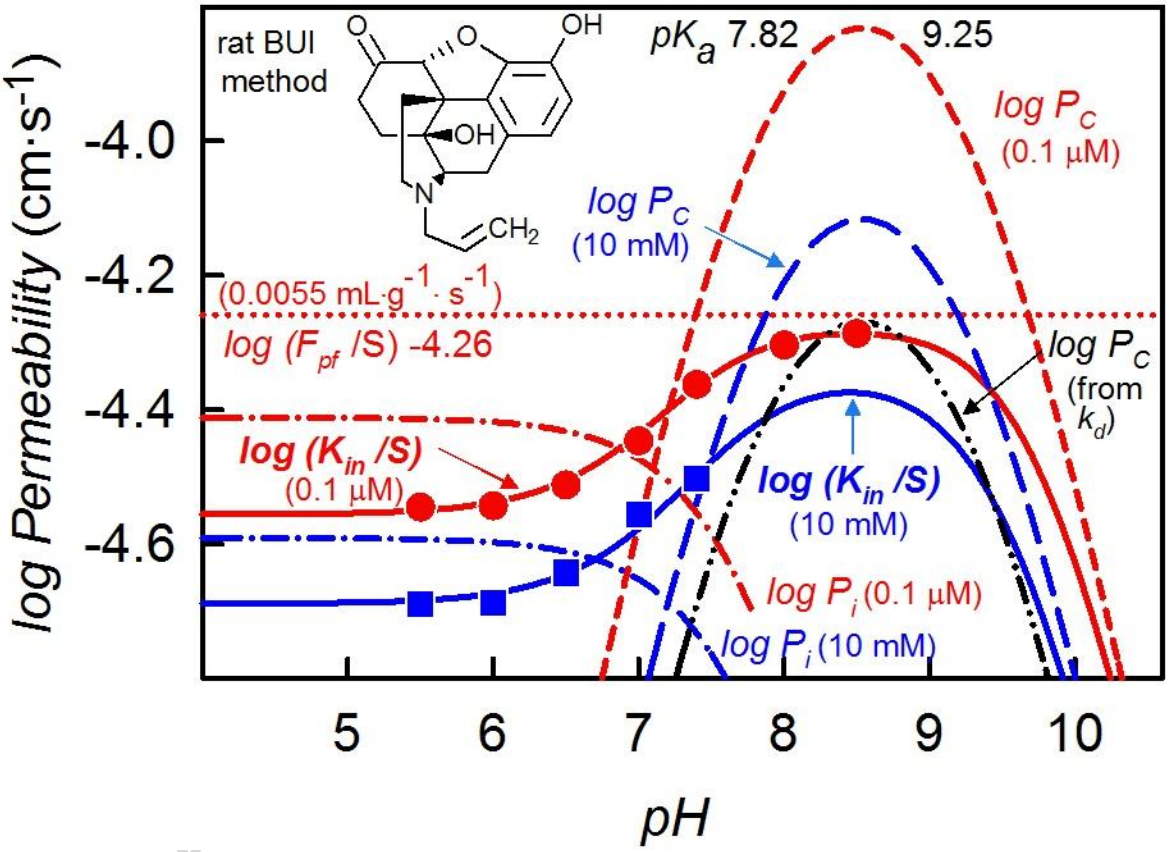

Figure 5

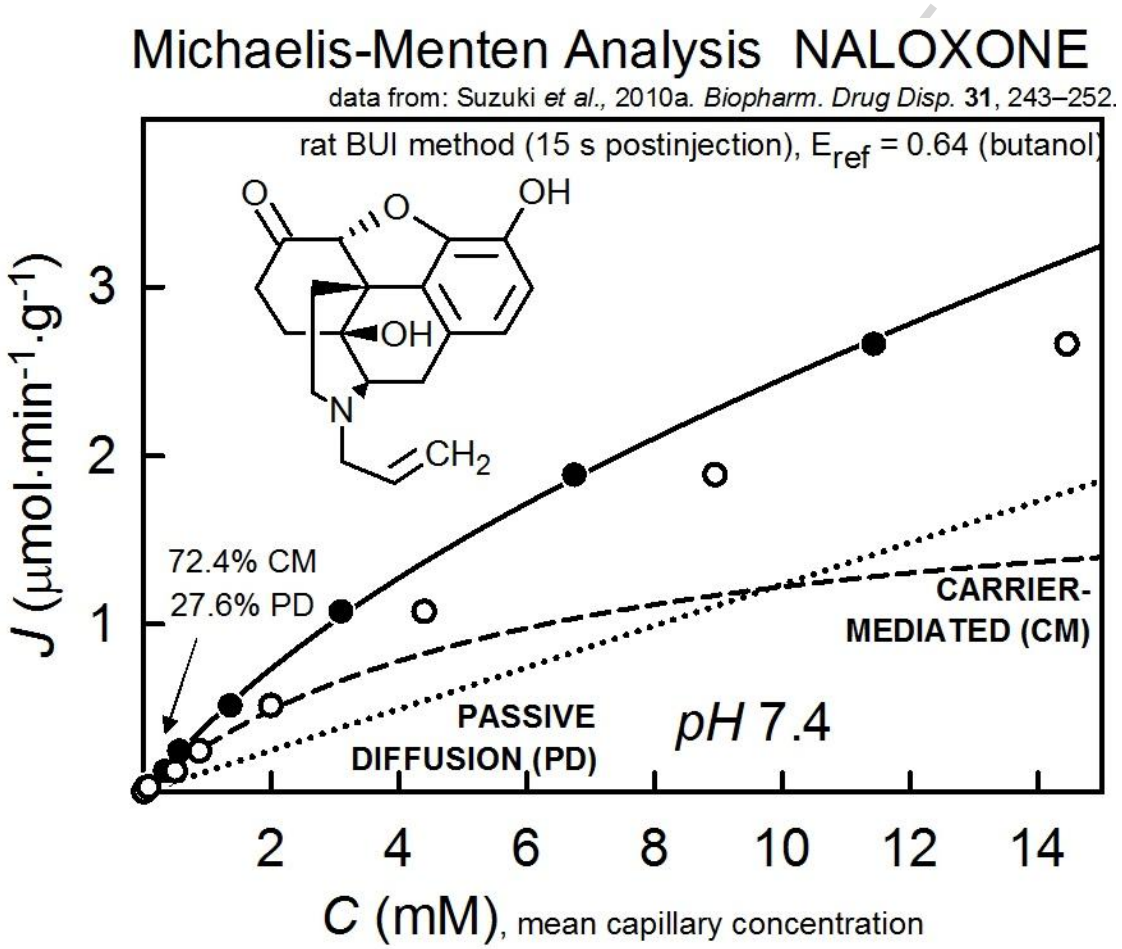

Figure 6

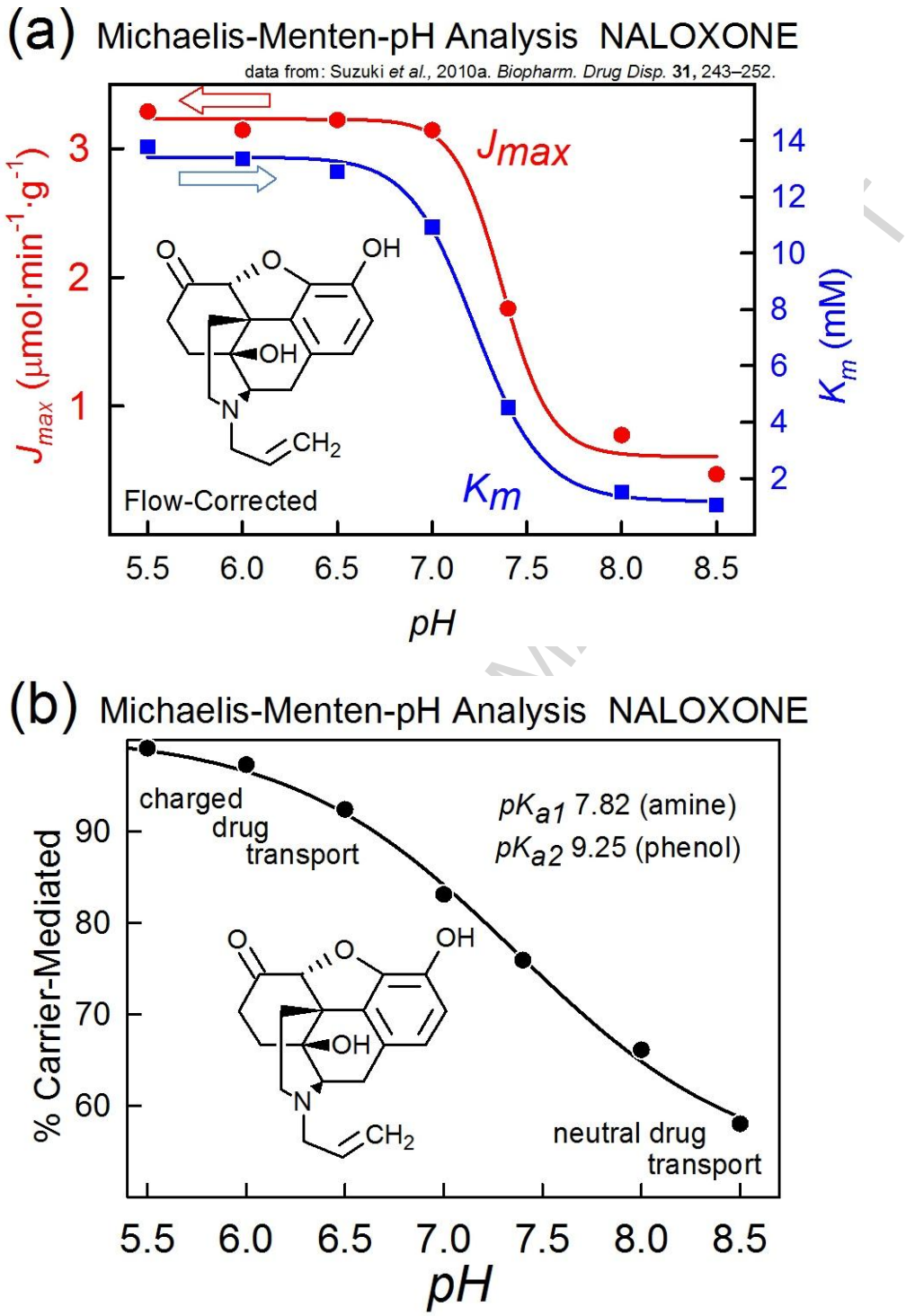

Figure 7

Graphical Abstract – Yusof et al.